

An all-frequency stable integral system for Maxwell's equations in 3-D penetrable media: continuous and discrete model analysis

Mahadevan Ganesh^{1*}, Stuart C. Hawkins² and Darko Volkov³

^{1*}Department of Applied Mathematics and Statistics, Colorado School of Mines, Golden, CO, USA.

²Department of Mathematical and Physical Sciences, Macquarie University, Sydney, NSW 2109, Australia.

³Department of Mathematical Sciences, Worcester Polytechnic Institute, Worcester, MA, USA.

*Corresponding author(s). E-mail(s): mganesh@mines.edu;
Contributing authors: stuart.hawkins@mq.edu.au; darko@wpi.edu;

Abstract

We introduce a new system of surface integral equations for Maxwell's transmission problem in three dimensions (3-D). This system has two remarkable features, both of which we prove. First, it is well-posed at all frequencies. Second, the underlying linear operator has a uniformly bounded inverse as the frequency approaches zero, ensuring that there is no low-frequency breakdown. The system is derived from a formulation we introduced in our previous work, which required additional integral constraints to ensure well-posedness across all frequencies. In this study, we eliminate those constraints and demonstrate that our new self-adjoint, constraints-free linear system—expressed in the desirable form of an identity plus a compact weakly-singular operator—is stable for all frequencies. Furthermore, we propose and analyze a fully discrete numerical method for these systems and provide a proof of spectrally accurate convergence for the computational method. We also computationally demonstrate the high-order accuracy of the algorithm using benchmark scatterers with curved surfaces.

Keywords: Electromagnetic scattering, dielectric, weakly singular integral equations, surface integral equations, stabilization, spectral numerical convergence

1 Introduction

Computation of the radar cross section (RCS) through simulation of electromagnetic waves in unbounded dielectric or absorbing penetrable media has been, and remains, crucial for advances in several technological and atmospheric science innovations [1–4]. The classical approach to modeling the electric and magnetic fields in the presence of a penetrable body in free space is based on the Maxwell partial differential equations (PDEs), augmented with a radiation condition for the exterior fields, and tangential continuity of the electric field and magnetizing field across the interface [5–7].

The Maxwell PDE system for the dielectric case has been proven to be uniquely solvable at all frequencies [8, 9]. As noted in the introduction of [10], this PDE system remains uniformly well-posed as the frequency approaches zero. This uniform well-posedness holds for the dielectric case, regardless of the scatterer’s genus. In contrast, for perfect conductors, additional conditions must be verified, as explained in [10]. This observation is consistent with the findings of the present authors in [11, Appendix B].

Our focus in this work is on time-harmonic electromagnetic waves with positive frequency ω , characterized in a three dimensional piecewise-constant medium by the electric field \mathcal{E} and magnetic field \mathcal{H} [7, Page 178] with

$$\mathcal{E}(\mathbf{x}, t) = \operatorname{Re} \{ \mathbf{E}(\mathbf{x}) e^{-i\omega t} \}, \quad \mathcal{H}(\mathbf{x}, t) = \operatorname{Re} \{ \mathbf{H}(\mathbf{x}) e^{-i\omega t} \}. \quad (1)$$

We denote by ∂D the boundary of a closed bounded region $D \subset \mathbb{R}^3$, and write $D^+ = \mathbb{R}^3 \setminus \overline{D}$ and $D^- = D$ for the exterior and interior of the penetrable domain D , respectively. The regularity of the electromagnetic field on the surface depends on the appropriate smoothness of the surface ∂D . We quantify such smoothness requirements in the first theorem of this article.

We denote the permittivity and permeability constants in D^\pm by ϵ^\pm and μ^\pm respectively. For the mathematical and numerical analysis of our new all-frequency stable formulation, we focus on non-plasmonic scatterers D . For such physical materials, following the literature [6, 7], we assume that μ^\pm and ϵ^+ are positive real numbers, and non-zero ϵ^- may be either a positive real number or a complex number with non-negative real and imaginary parts. Although our analyses may not apply to all cases involving real negative permittivity (such as the plasmonic case), the formulation and algorithm we present can still be utilized for a subset of plasmonic scenarios, which we will demonstrate in the last section of this article. In future work, we plan to develop mathematical and numerical analysis specifically for plasmonic materials.

It is convenient to then define

$$\epsilon(\mathbf{x}) = \epsilon^\pm, \quad \mu(\mathbf{x}) = \mu^\pm, \quad \text{for } \mathbf{x} \in D^\pm. \quad (2)$$

The refractive index of the medium is

$$\nu = \left(\frac{\mu^- \epsilon^-}{\mu^+ \epsilon^+} \right)^{1/2},$$

and the penetrable media is called dielectric when ν is real, and absorbing otherwise (in which case it follows from the assumptions above that the imaginary part of ν is positive).

Interaction of an incident electromagnetic field with the penetrable body D induces an interior field with spatial components $[\mathbf{E}^-, \mathbf{H}^-]$ in D^- and a scattered field with spatial components $[\mathbf{E}^+, \mathbf{H}^+]$ in D^+ . The spatial components $[\mathbf{E}, \mathbf{H}]$ of the induced field, with

$$\mathbf{E}(\mathbf{x}) = \mathbf{E}^\pm(\mathbf{x}), \quad \mathbf{H}(\mathbf{x}) = \mathbf{H}^\pm(\mathbf{x}), \quad \mathbf{x} \in D^\pm, \quad (3)$$

satisfy the time-harmonic Maxwell equations [7, Page 253]

$$\mathbf{curl} \mathbf{E}(\mathbf{x}) - i\omega\mu(\mathbf{x})\mathbf{H}(\mathbf{x}) = \mathbf{0}, \quad \mathbf{curl} \mathbf{H}(\mathbf{x}) + i\omega\epsilon(\mathbf{x})\mathbf{E}(\mathbf{x}) = \mathbf{0}, \quad \mathbf{x} \in D^\pm, \quad (4)$$

and the Silver-Müller radiation condition

$$\lim_{|\mathbf{x}| \rightarrow \infty} \left[\sqrt{\mu^+} \mathbf{H}(\mathbf{x}) \times \mathbf{x} - \sqrt{\epsilon^+} |\mathbf{x}| \mathbf{E}(\mathbf{x}) \right] = \mathbf{0}. \quad (5)$$

The exterior and interior fields are induced by an incident electromagnetic field $[\mathbf{E}_{\text{inc}}, \mathbf{H}_{\text{inc}}]$ impinging on the penetrable body. We require $[\mathbf{E}_{\text{inc}}, \mathbf{H}_{\text{inc}}]$ to satisfy the homogeneous Maxwell equations

$$\mathbf{curl} \mathbf{E}_{\text{inc}}(\mathbf{x}) - i\omega\mu^+ \mathbf{H}_{\text{inc}}(\mathbf{x}) = \mathbf{0}, \quad \mathbf{curl} \mathbf{H}_{\text{inc}}(\mathbf{x}) + i\omega\epsilon^+ \mathbf{E}_{\text{inc}}(\mathbf{x}) = \mathbf{0}, \quad \mathbf{x} \in \mathbb{R}^3 \setminus Q, \quad (6)$$

where $Q \subset \mathbb{R}^3$ is a compact or empty set, bounded away from the penetrable body D . In applications the incident wave is typically a plane wave, or a wave induced by a point source that satisfies (6). The total field is therefore $[\mathbf{E}_{\text{tot}}, \mathbf{H}_{\text{tot}}]$ with

$$\mathbf{E}_{\text{tot}}(\mathbf{x}) = \mathbf{E}_{\text{tot}}^\pm(\mathbf{x}), \quad \mathbf{H}_{\text{tot}}(\mathbf{x}) = \mathbf{H}_{\text{tot}}^\pm(\mathbf{x}), \quad \mathbf{x} \in D^\pm, \quad (7)$$

with

$$\mathbf{E}_{\text{tot}}^- = \mathbf{E}^-, \quad \mathbf{E}_{\text{tot}}^+ = \mathbf{E}^+ + \mathbf{E}_{\text{inc}}, \quad \mathbf{H}_{\text{tot}}^- = \mathbf{H}^-, \quad \mathbf{H}_{\text{tot}}^+ = \mathbf{H}^+ + \mathbf{H}_{\text{inc}}. \quad (8)$$

We highlight that inside D the total field is the induced field.

The tangential components of the total electric and magnetic fields are required to be continuous across the interface ∂D , leading to the interface conditions [7, Equation (5.6.66), Page 234]

$$\mathbf{E}_{\text{tot}}^- \times \mathbf{n} = \mathbf{E}_{\text{tot}}^+ \times \mathbf{n}, \quad \mathbf{H}_{\text{tot}}^- \times \mathbf{n} = \mathbf{H}_{\text{tot}}^+ \times \mathbf{n}, \quad \text{on } \partial D, \quad (9)$$

where \mathbf{n} is the outward unit normal to ∂D . A consequence of (4), (6), and (9) is that the normal components of the fields (called the surface charges) also satisfy interface conditions

$$\epsilon^- \mathbf{n} \cdot \mathbf{E}_{\text{tot}}^- = \epsilon^+ \mathbf{n} \cdot \mathbf{E}_{\text{tot}}^+, \quad \mu^- \mathbf{n} \cdot \mathbf{H}_{\text{tot}}^- = \mu^+ \mathbf{n} \cdot \mathbf{H}_{\text{tot}}^+, \quad \text{on } \partial D. \quad (10)$$

The scattered field $[\mathbf{E}^+, \mathbf{H}^+]$ has the asymptotic behavior of an outgoing spherical wave [6, Theorem 6.8, Page 164], and in particular,

$$\mathbf{E}^+(\mathbf{x}) = \frac{e^{ik_+|\mathbf{x}|}}{|\mathbf{x}|} \left\{ \mathbf{E}^\infty(\hat{\mathbf{x}}) + O\left(\frac{1}{|\mathbf{x}|}\right) \right\}, \quad (11)$$

as $|\mathbf{x}| \rightarrow \infty$ uniformly in all directions $\hat{\mathbf{x}} = \mathbf{x}/|\mathbf{x}|$, where $k_+ = \omega\sqrt{\mu^+\epsilon^+}$ is the exterior wavenumber. The vector field \mathbf{E}^∞ is known as the far field patterns of \mathbf{E}^+ .

One way to solve the Maxwell PDE system given by (4)–(10) is to formulate equivalent surface integral equations (SIEs) on ∂D . A key reason for reformulating the Maxwell PDEs as an SIE system is to facilitate the solution of the *unbounded* region model (4)–(10), through an equivalent model defined only on the *bounded* surface without truncation of the unbounded region and also satisfy the radiation condition at infinity exactly. In addition to the computational advantages of solving the 3-D Maxwell transmission problem using an SIE—where we only need to discretize for unknowns on the two-dimensional bounded surface—the surface integral operators in the SIE exhibit desirable boundedness and compactness properties compared to the unbounded differential operators in the PDEs. The foundational SIEs for non-spherical particles, known as the Electric Field Integral Equation (EFIE) and the Magnetic Field Integral Equation (MFIE), were proposed in Maue’s work from 1949 [12]. The issue of spurious resonances in these integral equations was addressed two decades later using a formulation known as the Combined Field Integral Equation (CFIE) [7]. The low-frequency breakdown problem in such SIEs has only been tackled in this century. In particular, for the dielectric model, all-frequency stable continuous and discrete formulations—subject to additional constraints—were first developed in [13, 14], which required the inversion of the surface Laplace–Beltrami differential operator. Subsequently, the authors presented further developments in [11, 15] with constraints on integral operators. However, those articles do not provide numerical analysis to mathematically quantify appropriate validity of the proposed discrete formulations.

In previous work [11] we discussed various classes of SIE for the Maxwell dielectric problem and introduced our own original formulation which was an integral equation combined with a stabilization constraint. We showed that this formulation possesses a few remarkable properties that, taken together, are unique: first, this system is in the classical form of the identity plus a compact operator. Second, it does not suffer from spurious eigenfrequencies. Third, it does not suffer from the low-frequency breakdown phenomenon: as the frequency tends to zero, this system remains uniformly well posed. Fourth, the solution to combined system is equal to the trace of the electric and magnetic fields on the interface.

All these four points were established in [11], subject to the non-plasmonic regime parameters assumptions described earlier. For the entire plasmonic regime, we are not aware of any SIE formulation in the literature that has been proven or even numerically demonstrated to exhibit all these four remarkable features. In the case of the plasmonic regime, as we numerically demonstrate in Section 6, and as also shown in [16] for several other SIE formulations, it is plausible that these four features may hold only for a subset of parameters within the plasmonic region. We plan to explore

and quantify such a subset region through mathematical and numerical analysis in future work.

The main focus of this article, for the non-plasmonic region, is to implement the stabilization derived in [11] in such a way that a high-order numerical method can be developed, and prove spectral convergence of the numerical algorithm. To this end, one of the main issues is how to incorporate the stabilization into the integral equation formulation and retain an all-frequency stable uniquely-solvable system. One of the established approaches, as in the traditional CFIE (combining the EFIE and MFIE) is to take a linear combination of the integral equation and the stabilization constraint. Such an approach has been used in the engineering literature [17, 18] without any proof that the uniquely solvable property is retained for all frequencies. We used such an approach for preliminary numerical investigations in [11] and demonstrated that, for spherical scatterers, there are some coupling parameters for which the unique solvability cannot be guaranteed for all frequencies. One of the key contributions in this present work is to establish, using robust mathematical proofs, that such a simple one-parameter coupling approach will lead to a non-uniquely solvable system for infinitely many choices of the parameters. Accordingly, using such a simple approach does not guarantee, in general, the key properties of the all-frequency stable integral equation formulation, subject to the constraint.

Subsequently, in this article we introduce a new continuous formulation that incorporates the constraint efficiently into one equation, and we prove that the established unique solution, with the constraint, is equivalent to the solution obtained using our new coupled formulation. The main focus of this paper is to apply a high-order numerical algorithm for the new symmetric formulation, and prove spectrally accurate convergence under certain conditions that are especially suited for curved interfaces. We substantiate our robust mathematical results with numerical experiments. The underlying spectrally-accurate numerical framework was developed for perfect conductors in [19] and subsequently further developed for the dielectric model in [15], where we incorporated the constraint using a complicated saddle-point formulation. Numerical analysis of such a saddle-point approach is yet to be explored. The present article is the first work in the literature to develop numerical analysis for an all-frequency stable and uniquely solvable weakly-singular SIE system.

The rest of this article is as follows:

- In Section 2 we first review properties of surface integral operators that are relevant to this study.
- We then review an all-frequency stable surface integral equation subject to a stabilization constraint, and a main result from [11] in Section 3.
- In Appendix A we prove that the simple approach of combining the integral equation with the stabilization constraint using a single parameter does not, in general, guarantee unique solvability of the resulting system, for infinitely many choices of the parameters.
- Motivated by this, in Section 4 we introduce a new equivalent formulation incorporating the stabilization constraint in a self-adjoint form and prove that the new single-equation system, without any constraint, is uniquely solvable.

- In Section 5 we introduce a fully-discrete numerical scheme for our new single-equation weakly-singular SIE system and prove that the associated numerical solution converges super-algebraically.
- In Section 6 we implement the spectrally accurate algorithm and demonstrate the superalgebraic convergence for a class of convex and non-convex test obstacles that are widely used in the literature.

2 Surface integral operators and properties

In this section we introduce the integral operators that subsequently appear in our SIE. The starting point is the use of particular potentials and their traces onto the interface ∂D . We use the same notation as in our previous article [11] and we first recall from [11] some notation and definitions. For related derivations and proofs, we refer to [11].

Let $\Omega \subseteq \mathbb{R}^3$ be either D^- , D^+ , ∂D or \mathbb{R}^3 . For a non-negative integer m and $\sigma \in \mathbb{R}$ with $0 < \sigma \leq 1$, let $C^m(\overline{\Omega})$ denote the standard space of m -times continuously differentiable functions and $C^{m,\sigma}(\overline{\Omega})$ denote the Hölder space of all functions in $C^m(\overline{\Omega})$ whose derivatives of order m are uniformly Hölder continuous with exponent σ . For $s \in \mathbb{R}$ and bounded Ω the space $H^s(\Omega)$ is the standard Sobolev space of order s .

The vector-valued counterparts of these spaces will be denoted by boldface symbols. Thus, for $m \in \mathbb{N}$, $s \in \mathbb{R}$, $0 \leq \sigma \leq 1$,

$$\mathbf{C}^{m,\sigma}(\overline{\Omega}) = \left[C^{m,\sigma}(\overline{\Omega}) \right]^3, \quad \mathbf{H}^s(\Omega) = \left[H^s(\Omega) \right]^3. \quad (12)$$

Let γ^\pm be the standard exterior/interior trace operator defined for a continuous vector field \mathbf{u} on $\overline{D^\pm}$ as

$$\left(\gamma^\pm \mathbf{u} \right)(\mathbf{x}) = \lim_{h \rightarrow 0^\pm} \mathbf{u}(\mathbf{x} + h\mathbf{n}(\mathbf{x})), \quad \mathbf{x} \in \partial D. \quad (13)$$

Let $\gamma_t^\pm, \gamma_n^\pm$ be respectively the (twisted) tangential and normal trace operators, defined for a continuous vector field \mathbf{u} on $\overline{D^\pm}$ as

$$\gamma_t^\pm \mathbf{u} = (\gamma^\pm \mathbf{u}) \times \mathbf{n}, \quad \gamma_n^\pm \mathbf{u} = (\gamma^\pm \mathbf{u}) \cdot \mathbf{n}. \quad (14)$$

We denote by $\mathbf{C}_t^{m,\sigma}(\partial D)$ and $\mathbf{H}_t^s(\partial D)$ respectively the spaces of tangential vector fields on ∂D with regularity $\mathbf{C}^{m,\sigma}$ and \mathbf{H}^s .

Let

$$G_\pm(\mathbf{x}, \mathbf{y}) = \frac{1}{4\pi} \frac{e^{ik_\pm |\mathbf{x}-\mathbf{y}|}}{|\mathbf{x}-\mathbf{y}|}, \quad (15)$$

where $k_\pm = \omega \sqrt{\epsilon^\pm \mu^\pm}$ denotes the exterior and interior wavenumber respectively. Let Ψ_\pm^V and $\underline{\Psi}_\pm^V$ be respectively the scalar and vector single layer potential operators,

defined for scalar and vector surface densities w and \mathbf{w} as

$$(\Psi_{\pm}^V w)(\mathbf{x}) = \int_{\partial D} G_{\pm}(\mathbf{x}, \mathbf{y}) w(\mathbf{y}) ds(\mathbf{y}), \quad (\underline{\Psi}_{\pm}^V \mathbf{w})(\mathbf{x}) = \int_{\partial D} G_{\pm}(\mathbf{x}, \mathbf{y}) \mathbf{w}(\mathbf{y}) ds(\mathbf{y}), \quad (16)$$

for $\mathbf{x} \in \mathbb{R}^3 \setminus \partial D$. We assume that the surface ∂D is at least of class $C^{m^*,1}$, for some integer $m^* \geq 1$. Then the operators $\Psi_{\pm}^V : C(\partial D) \rightarrow C^{0,\alpha}(\mathbb{R}^3)$ and, for $0 < \alpha < 1$, $\underline{\Psi}_{\pm}^V : \mathbf{C}(\partial D) \rightarrow \mathbf{C}^{0,\alpha}(\mathbb{R}^3)$ are bounded linear operators [6, Theorems 3.3, 6.12]. Hence $\gamma_{\mathbf{t}}^{\pm} \circ \underline{\Psi}_{\pm}^V : \mathbf{C}(\partial D) \rightarrow \mathbf{C}_t^{0,\alpha}(\partial D)$ is a bounded linear operator and consequently compact as an operator onto $\mathbf{C}(\partial D)$ because of the compact imbedding [6, Theorem 3.2]. Similarly, using the properties of the single layer potential on Sobolev spaces (see [20, Theorem 1(i)]), $\gamma_{\mathbf{t}}^{\pm} \circ \underline{\Psi}_{\pm}^V$ is a compact operator onto $\mathbf{H}^{\frac{1}{2}}(\partial D)$. Using the jump relation for the single layer potential [6, 7], we obtain

$$\gamma_{\mathbf{t}}^{\pm} \circ \underline{\Psi}_{\pm}^V \mathbf{w} = \underline{\mathcal{A}}_{\pm} \mathbf{w}, \quad \gamma_{\mathbf{n}}^{\pm} \circ \underline{\Psi}_{\pm}^V \mathbf{w} = \mathcal{F}_{\pm} \mathbf{w}, \quad (17)$$

where the tangential-field-valued and scalar-valued operators are defined as

$$(\underline{\mathcal{A}}_{\pm} \mathbf{w})(\mathbf{x}) = \int_{\partial D} G_{\pm}(\mathbf{x}, \mathbf{y}) \mathbf{w}(\mathbf{y}) \times \mathbf{n}(\mathbf{x}) ds(\mathbf{y}), \quad \mathbf{x} \in \partial D, \quad (18)$$

$$(\mathcal{F}_{\pm} \mathbf{w})(\mathbf{x}) = \int_{\partial D} G_{\pm}(\mathbf{x}, \mathbf{y}) \mathbf{w}(\mathbf{y}) \cdot \mathbf{n}(\mathbf{x}) ds(\mathbf{y}), \quad \mathbf{x} \in \partial D. \quad (19)$$

It is useful to consider the normal-field operator

$$(\mathbf{n}\mathcal{F}_{\pm} \mathbf{w})(\mathbf{x}) = \mathbf{n}(\mathbf{x})(\mathcal{F}_{\pm} \mathbf{w})(\mathbf{x}), \quad \mathbf{x} \in \partial D. \quad (20)$$

The surface integral operators $\underline{\mathcal{A}}_{\pm}$ and $\mathbf{n}\mathcal{F}_{\pm}$ are compact as operators on $\mathbf{C}(\partial D)$ and $\mathbf{H}^{\frac{1}{2}}(\partial D)$. Further, for α , s and integer m satisfying

$$0 < \alpha < 1, \quad 0 \leq m < m^*, \quad 0 < s \leq m^*, \quad (21)$$

we have that

$$\underline{\mathcal{A}}_{\pm}, \mathbf{n}\mathcal{F}_{\pm} : \mathbf{C}^m(\partial D) \rightarrow \mathbf{C}^{m,\alpha}(\partial D), \quad \underline{\mathcal{A}}_{\pm}, \mathbf{n}\mathcal{F}_{\pm} : \mathbf{H}^{s-1}(\partial D) \rightarrow \mathbf{H}^s(\partial D), \quad (22)$$

are bounded linear operators. The operators in (18)–(20) enjoy these smoothing (and hence compactness) properties essentially because the kernels of these surface integral operators are weakly-singular.

We define vector-valued surface integral operators

$$(\underline{\mathcal{B}}_{\pm} \mathbf{w})(\mathbf{x}) = \int_{\partial D} \mathbf{grad}_{\mathbf{x}} G_{\pm}(\mathbf{x}, \mathbf{y}) \times \mathbf{n}(\mathbf{x}) w(\mathbf{y}) ds(\mathbf{y}), \quad (23)$$

$$(\underline{\mathcal{C}}_{\pm} \mathbf{w})(\mathbf{x}) = -\mathbf{n}(\mathbf{x}) \times \mathbf{curl}_{\mathbf{x}} \int_{\partial D} G_{\pm}(\mathbf{x}, \mathbf{y}) \mathbf{w}(\mathbf{y}) ds(\mathbf{y}), \quad (24)$$

for $\mathbf{x} \in \partial D$, and related scalar-valued surface integral operators

$$(\mathcal{G}_\pm w)(\mathbf{x}) = \int_{\partial D} \frac{\partial G_\pm}{\partial \mathbf{n}(\mathbf{x})}(\mathbf{x}, \mathbf{y}) w(\mathbf{y}) ds(\mathbf{y}), \quad (25)$$

$$(\mathcal{H}_\pm w)(\mathbf{x}) = \int_{\partial D} \left(\mathbf{grad}_x G_\pm(\mathbf{x}, \mathbf{y}) \times \mathbf{n}(\mathbf{x}) \right) \cdot w(\mathbf{y}) ds(\mathbf{y}). \quad (26)$$

We note that for a tangential density w ,

$$(\underline{\mathcal{C}}_\pm w)(\mathbf{x}) = (\underline{\mathcal{D}}_\pm w)(\mathbf{x}) - (\underline{\mathcal{E}}_\pm w)(\mathbf{x}), \quad (27)$$

where for $\mathbf{x} \in \partial D$,

$$(\underline{\mathcal{D}}_\pm w)(\mathbf{x}) = \int_{\partial D} \frac{\partial G_\pm}{\partial \mathbf{n}(\mathbf{x})}(\mathbf{x}, \mathbf{y}) w(\mathbf{y}) ds(\mathbf{y}), \quad (28)$$

$$(\underline{\mathcal{E}}_\pm w)(\mathbf{x}) = \int_{\partial D} \left(\mathbf{grad}_x G_\pm(\mathbf{x}, \mathbf{y}) \right) w(\mathbf{y}) \cdot \left(\mathbf{n}(\mathbf{x}) - \mathbf{n}(\mathbf{y}) \right) ds(\mathbf{y}). \quad (29)$$

It is also useful to consider the normal field surface integral operators

$$(\mathbf{n}\mathcal{G}_\pm w)(\mathbf{x}) = \mathbf{n}(\mathbf{x})(\mathcal{G}_\pm w)(\mathbf{x}), \quad (\mathbf{n}\mathcal{H}_\pm w)(\mathbf{x}) = \mathbf{n}(\mathbf{x})(\mathcal{H}_\pm w)(\mathbf{x}), \quad \mathbf{x} \in \partial D. \quad (30)$$

Clearly, the kernels of the surface integral operators $\underline{\mathcal{D}}_\pm$ and \mathcal{G}_\pm are weakly-singular. Hence \mathcal{G}_\pm is a compact operator on $C(\partial D)$ and $\mathbf{H}^{\frac{1}{2}}(\partial D)$.

Since ∂D is of at least $C^{1,1}$ -class, we obtain

$$|\mathbf{n}(\mathbf{x}) - \mathbf{n}(\mathbf{y})| \leq C|\mathbf{x} - \mathbf{y}|, \quad \mathbf{x}, \mathbf{y} \in \partial D, \quad (31)$$

for some constant C that depends on the geometry of ∂D . Thus, because of the term $\mathbf{n}(\mathbf{x}) - \mathbf{n}(\mathbf{y})$ in (29), the operator $\underline{\mathcal{E}}_\pm$ is weakly-singular. There is a vast amount of literature [21–23] explaining that this implies that $\underline{\mathcal{C}}_\pm$ is a compact operator on $\mathbf{C}_t(\partial D)$ and on $\mathbf{H}_t^{\frac{1}{2}}(\partial D)$. In addition, if (21) holds then

$$\begin{aligned} \underline{\mathcal{C}}_\pm &: \mathbf{C}_t^m(\partial D) \rightarrow \mathbf{C}_t^{m,\alpha}(\partial D), & \underline{\mathcal{C}}_\pm &: \mathbf{H}_t^{s-1}(\partial D) \rightarrow \mathbf{H}_t^s(\partial D), \\ \mathcal{G}_\pm &: C^m(\partial D) \rightarrow C^{m,\alpha}(\partial D), & \mathcal{G}_\pm &: H^{s-1}(\partial D) \rightarrow H^s(\partial D), \end{aligned}$$

are bounded linear operators. The kernels of the surface integral operators $\underline{\mathcal{B}}_\pm, \mathcal{H}_\pm$ in (23), (26) have order $1/r^2$ singularity. However, our reformulation of the time-harmonic dielectric model requires only operators $\underline{\mathcal{B}}_+ - \underline{\mathcal{B}}_-$ and $\mathcal{H}_+ - \mathcal{H}_-$. It follows from [24, Remark 3.1.3] that $\underline{\mathcal{B}}_+ - \underline{\mathcal{B}}_-$ and $\mathcal{H}_+ - \mathcal{H}_-$ have weakly-singular kernels. Thus the operator $\mathbf{n}\mathcal{H}_+ - \mathbf{n}\mathcal{H}_-$ is compact on $\mathbf{C}(\partial D)$ and $\mathbf{H}^{\frac{1}{2}}(\partial D)$ whilst the operator $\underline{\mathcal{B}}_+ - \underline{\mathcal{B}}_-$ is compact on $C(\partial D)$ and $H^{\frac{1}{2}}(\partial D)$, and if (21) holds then the following linear operators are bounded:

$$\mathbf{n}\mathcal{H}_+ - \mathbf{n}\mathcal{H}_- : \mathbf{C}^m(\partial D) \rightarrow \mathbf{C}^{m,\alpha}(\partial D), \quad \mathbf{n}\mathcal{H}_+ - \mathbf{n}\mathcal{H}_- : \mathbf{H}^{s-1}(\partial D) \rightarrow \mathbf{H}^s(\partial D),$$

$$\underline{\mathbf{B}}_+ - \underline{\mathbf{B}}_- : C^m(\partial D) \rightarrow C^{m,\alpha}(\partial D), \quad \underline{\mathbf{B}}_+ - \underline{\mathbf{B}}_- : \mathbf{H}^{s-1}(\partial D) \rightarrow \mathbf{H}^s(\partial D).$$

Furthermore, we define two further scalar integral operators that we use in our additional scalar integral equations for indirectly imposing the identities connecting currents and charges,

$$(\mathcal{S}_\pm w)(\mathbf{x}) = \int_{\partial D} G_\pm(\mathbf{x}, \mathbf{y}) w(\mathbf{y}) ds(\mathbf{y}), \quad \mathbf{x} \in \partial D, \quad (32)$$

$$(\mathcal{K}_\pm \mathbf{w})(\mathbf{x}) = \int_{\partial D} \left(\mathbf{grad}_x G_\pm(\mathbf{x}, \mathbf{y}) \times \mathbf{n}(\mathbf{y}) \right) \cdot \mathbf{w}(\mathbf{y}) ds(\mathbf{y}), \quad \mathbf{x} \in \partial D. \quad (33)$$

The operator $\mathcal{S}_+ - \mathcal{S}_-$ is compact on $C(\partial D)$ and $\mathbf{H}^{\frac{1}{2}}(\partial D)$ whilst the operator $\mathcal{K}_+ - \mathcal{K}_-$ is compact on $C(\partial D)$ and $\mathbf{H}^{\frac{1}{2}}(\partial D)$, and if (21) holds then the following linear operators are bounded:

$$\begin{aligned} \mathcal{S}_+ - \mathcal{S}_- : C^m(\partial D) &\rightarrow C^{m,\alpha}(\partial D), & \mathcal{S}_+ - \mathcal{S}_- : \mathbf{H}^{s-1}(\partial D) &\rightarrow \mathbf{H}^s(\partial D), \\ \mathcal{K}_+ - \mathcal{K}_- : C^m(\partial D) &\rightarrow C^{m,\alpha}(\partial D), & \mathcal{K}_+ - \mathcal{K}_- : \mathbf{H}^{s-1}(\partial D) &\rightarrow \mathbf{H}^s(\partial D). \end{aligned}$$

Finally, we introduce the following weakly-singular operators to facilitate recalling in the next section our first second-kind surface-integral system that is all-frequency-stable subject to a stability constraint.

$$\begin{aligned} \tilde{\underline{\mathbf{C}}}^{(\alpha^+, \alpha^-)} &= \alpha^+ \underline{\mathbf{C}}_+ - \alpha^- \underline{\mathbf{C}}_-, & \tilde{\underline{\mathbf{A}}}^{(\alpha^+, \alpha^-, \beta^+, \beta^-, \lambda)} &= i\lambda(\beta^+ \alpha^+ \underline{\mathbf{A}}_+ - \beta^- \alpha^- \underline{\mathbf{A}}_-), \\ \tilde{\mathcal{G}}^{(\alpha^+, \alpha^-)} &= \mathcal{G}_+ - \frac{\alpha^+}{\alpha^-} \mathcal{G}_-, & \tilde{\mathcal{F}}^{(\alpha^+, \alpha^-, \lambda)} &= i\lambda(\alpha^+ \mathcal{F}_+ - \alpha^- \mathcal{F}_-), \\ \tilde{\underline{\mathbf{B}}} &= \underline{\mathbf{B}}_+ - \underline{\mathbf{B}}_-, & \tilde{\mathcal{H}} &= \mathcal{H}_+ - \mathcal{H}_-, & \tilde{\mathcal{S}} &= (\mathcal{S}_+ - \mathcal{S}_-), & \tilde{\mathcal{K}} &= (\mathcal{K}_+ - \mathcal{K}_-). \end{aligned} \quad (34)$$

In this notation, when it is used subsequently, the parameter λ will be replaced by $\pm\omega$ and hence $\tilde{\underline{\mathbf{A}}}^{(\alpha^+, \alpha^-, \beta^+, \beta^-, \pm\omega)}$ and $\tilde{\mathcal{F}}^{(\alpha^+, \alpha^-, \pm\omega)}$ tend to zero operators as $\omega \rightarrow 0$.

3 A stability constrained well-posed SIE system

In this section we recall from [11] a matrix-operator and a stability constraint, and hence, subject to the constraint, an all-frequency-stable weakly-singular SIE system that is equivalent to the Maxwell PDE. To this end, let \mathbb{M} be the 2×2 weakly-singular operator

$$\mathbb{M} = \begin{bmatrix} \mathcal{M}^{(\epsilon^+, \epsilon^-)} & \mathcal{N}^{(\epsilon^+, \epsilon^-, \mu^+, \mu^-, \omega)} \\ \mathcal{N}^{(\mu^+, \mu^-, \epsilon^+, \epsilon^-, -\omega)} & \mathcal{M}^{(\mu^+, \mu^-)} \end{bmatrix}, \quad (35)$$

with

$$\mathcal{M}^{(\alpha^+, \alpha^-)} \mathbf{w} = \frac{2}{\alpha^+ + \alpha^-} \left\{ \mathbf{n} \times \left[\tilde{\underline{\mathbf{C}}}^{(\alpha^+, \alpha^-)} (\mathbf{w} \times \mathbf{n}) + \alpha^+ \tilde{\underline{\mathbf{B}}} (\mathbf{w} \cdot \mathbf{n}) \right] \right\}$$

$$-\alpha^- \mathbf{n} \left[\tilde{\mathcal{H}}(\mathbf{w} \times \mathbf{n}) - \tilde{\mathcal{G}}^{(\alpha^+, \alpha^-)}(\mathbf{w} \cdot \mathbf{n}) \right] \Big\}, \quad (36)$$

$$\mathcal{N}^{(\alpha^+, \alpha^-, \beta^+, \beta^-, \lambda)} \mathbf{w} = \frac{2}{\alpha^+ + \alpha^-} \left\{ \left[\mathbf{n} \times \tilde{\mathcal{A}}^{(\alpha^+, \alpha^-, \beta^+, \beta^-, \lambda)} + \alpha^- \mathbf{n} \tilde{\mathcal{F}}^{(\beta^+, \beta^-, \lambda)} \right] (\mathbf{w} \times \mathbf{n}) \right\}. \quad (37)$$

It is easy to see the important property of \mathbb{M} that in the limit $\omega \rightarrow 0$, the off-diagonal entries of \mathbb{M} are zero, and hence the resulting diagonal operator facilitates decoupling of the electric and magnetic fields as $\omega \rightarrow 0$. We further observe that, because of the weak singularity of their kernels, $\mathcal{M}^{(\alpha_+, \alpha_-)}$ and $\mathcal{N}^{(\alpha_+, \alpha_-, \beta_+, \beta_-, \lambda)}$ defined in (36)–(37) are compact as operators on $X, \mathbf{C}(\partial D)$ and on $\mathbf{H}^{\frac{1}{2}}(\partial D)$. Furthermore, for α , m and s satisfying (21),

$$\begin{aligned} \mathcal{M}^{(\alpha_+, \alpha_-)}, \mathcal{N}^{(\alpha_+, \alpha_-, \beta_+, \beta_-, \lambda)} &: \mathbf{C}^m(\partial D) \rightarrow \mathbf{C}^{m, \alpha}(\partial D), \\ \mathcal{M}^{(\alpha_+, \alpha_-)}, \mathcal{N}^{(\alpha_+, \alpha_-, \beta_+, \beta_-, \lambda)} &: \mathbf{H}^{s-1}(\partial D) \rightarrow \mathbf{H}^s(\partial D), \end{aligned}$$

are bounded linear operators. Consequently the 2×2 matrix-operator \mathbb{M} defined in (35) is a compact operator on $\mathbf{C}(\partial D) \times \mathbf{C}(\partial D)$ and on $\mathbf{H}^{\frac{1}{2}}(\partial D) \times \mathbf{H}^{\frac{1}{2}}(\partial D)$. In addition, if (21) holds then

$$\mathbb{M} : \mathbf{C}^m(\partial D) \times \mathbf{C}^m(\partial D) \rightarrow \mathbf{C}^{m, \alpha}(\partial D) \times \mathbf{C}^{m, \alpha}(\partial D), \quad (38)$$

$$\mathbb{M} : \mathbf{H}^{s-1}(\partial D) \times \mathbf{H}^{s-1}(\partial D) \rightarrow \mathbf{H}^s(\partial D) \times \mathbf{H}^s(\partial D), \quad (39)$$

are bounded linear operators. For $\mathbf{x} \in \partial D$ define,

$$\mathbf{e}^i(\mathbf{x}) = \frac{2\epsilon^+}{\epsilon^+ + \epsilon^-} \mathbf{n}(\mathbf{x}) \times (\boldsymbol{\gamma}_t^+ \mathbf{E}_i)(\mathbf{x}) + \frac{2\epsilon^-}{\epsilon^+ + \epsilon^-} \mathbf{n}(\mathbf{x}) (\boldsymbol{\gamma}_n^+ \mathbf{E}_i)(\mathbf{x}), \quad (40)$$

$$\mathbf{h}^i(\mathbf{x}) = \frac{2\mu^+}{\mu^+ + \mu^-} \mathbf{n}(\mathbf{x}) \times (\boldsymbol{\gamma}_t^+ \mathbf{H}_i)(\mathbf{x}) + \frac{2\mu^-}{\mu^+ + \mu^-} \mathbf{n}(\mathbf{x}) (\boldsymbol{\gamma}_n^+ \mathbf{H}_i)(\mathbf{x}), \quad (41)$$

where $[\mathbf{E}_i, \mathbf{H}_i]$ is an incident electromagnetic wave. In [11] we proved that $(\mathbf{f}, \mathbf{g})^T = (\mathbf{e}^i, \mathbf{h}^i)^T$ and $(\mathbf{e}, \mathbf{h})^T$ is the exterior trace of the total field solving the Maxwell dielectric problem (4)–(10) for the same incident field $[\mathbf{E}_i, \mathbf{H}_i]$, then

$$[\mathbb{I} + \mathbb{M}] \begin{pmatrix} \mathbf{e} \\ \mathbf{h} \end{pmatrix} = \begin{pmatrix} \mathbf{f} \\ \mathbf{g} \end{pmatrix}, \quad (42)$$

where \mathbb{I} is the block identity operator. This holds for all frequencies $\omega > 0$. *However, the system (42) may become singular for some frequencies ω .* In [11] we found a constraint such that equation (42) augmented by that constraint is uniquely solvable for all frequencies. The stability constraint, which actually uses just scalar operators that are also used in acoustics, is governed by the operator \mathbb{J} defined (with the same domain

and range spaces as \mathbb{M}) as:

$$\mathbb{J} \begin{pmatrix} \tilde{\mathbf{e}} \\ \tilde{\mathbf{h}} \end{pmatrix} = \left(0, 0, \tilde{\mathcal{K}}\tilde{\mathbf{e}} + i\omega\mu^+\tilde{\mathcal{S}}(\tilde{\mathbf{h}} \cdot \mathbf{n}), 0, 0, \tilde{\mathcal{K}}\tilde{\mathbf{h}} - i\omega\epsilon^+\tilde{\mathcal{S}}(\tilde{\mathbf{e}} \cdot \mathbf{n}) \right)^T. \quad (43)$$

For α , m and s satisfying (21),

$$\mathbb{J} : \mathbf{C}^m(\partial D) \times \mathbf{C}^m(\partial D) \rightarrow \mathbf{C}^{m,\alpha}(\partial D) \times \mathbf{C}^{m,\alpha}(\partial D), \quad (44)$$

$$\mathbb{J} : \mathbf{H}^{s-1}(\partial D) \times \mathbf{H}^{s-1}(\partial D) \rightarrow \mathbf{H}^s(\partial D) \times \mathbf{H}^s(\partial D), \quad (45)$$

are bounded linear operators. Similar to \mathbb{M} , as $\omega \rightarrow 0$ the electric and magnetic fields are decoupled in the range of the stabilization operator \mathbb{J} . We now state the main result on the well-posedness of the stabilized SIE model.

Theorem 1. *Let $[\mathbf{f}, \mathbf{g}]^T$ be the trace on ∂D of some incident field $[\mathbf{E}_{\text{inc}}, \mathbf{H}_{\text{inc}}]$. Assume that ϵ^\pm and μ^\pm are as specified in Section 1. Let $[\mathbf{E}, \mathbf{H}]$ be the unique solution of the associated penetrable scattering model (4)–(9). Then $[\mathbf{e}, \mathbf{h}] = [\gamma^+ \mathbf{E}_{\text{tot}}^+, \gamma^+ \mathbf{H}_{\text{tot}}^+]$ is the **unique** solution of the weakly-singular SIE*

$$[\mathbb{I} + \mathbb{M}] \begin{pmatrix} \mathbf{e} \\ \mathbf{h} \end{pmatrix} = \begin{pmatrix} \mathbf{f} \\ \mathbf{g} \end{pmatrix}, \text{ subject to } \mathbb{J} \begin{pmatrix} \mathbf{e} \\ \mathbf{h} \end{pmatrix} = \begin{pmatrix} \mathbf{0} \\ \mathbf{0} \end{pmatrix}. \quad (46)$$

In addition, if ∂D is of class $C^{m,1}$ with $m \geq 1$, then $(\mathbf{e}, \mathbf{h})^T \in \mathbf{C}^{m-1,1}(\partial D) \times \mathbf{C}^{m-1,1}(\partial D)$ and depends continuously on $(\mathbf{f}, \mathbf{g})^T$. Also $(\mathbf{e}, \mathbf{h})^T \in \mathbf{H}^m(\partial D) \times \mathbf{H}^m(\partial D)$ and depends continuously on $(\mathbf{f}, \mathbf{g})^T$.

Proof. See [11]. □

4 A self-adjoint SIE system without constraints: well-posedness and low frequency stability

If the operator $\mathbb{I} + \mathbb{M}$ is singular, then instead of solving equation (42), we could instead substitute $\mathbb{I} + \mathbb{M} + \xi\mathbb{J}$ for $\mathbb{I} + \mathbb{M}$, for a fixed complex number ξ that would produce a regular operator (that is, a continuous operator with continuous inverse). This is reasonable because for right hand sides of interest, derived from incident waves, we desire solutions $[\mathbf{e}, \mathbf{h}]$ that satisfy the constraint $\mathbb{J}(\mathbf{e}, \mathbf{h})^T = (\mathbf{0}, \mathbf{0})^T$. Unfortunately, however, we do not know a-priori what value to choose for ξ . Once ξ is fixed, if ω is changed then the resulting operator $\mathbb{I} + \mathbb{M} + \xi\mathbb{J}$ may become singular. This was demonstrated numerically in [11] for a spherical scatterer and, in fact, we show in Appendix A that this approach may fail for *any choice* of the complex scalar ξ .

More generally, solving linear problems with constraints has been an area of interest for a long time and is surveyed in [25]. However, none of the cases covered in that survey paper applies to our particular case. This is chiefly due to the fact that \mathbb{M} is not symmetric, and that it is important for us not to lose the “identity plus compact” form of our operator.

Each of the operators introduced in Section 2 has a formal adjoint, and it is easy to verify that the adjoint operators \mathbb{M}^* and \mathbb{J}^* satisfy the same continuity properties as \mathbb{M} and \mathbb{J} . To describe the continuity properties of \mathbb{M} , \mathbb{J} and their adjoints, it is helpful to introduce the following notations: the space $\mathbf{C}_2(\partial D)$ will be defined to be the product space $\mathbf{C}(\partial D) \times \mathbf{C}(\partial D)$. $\mathbf{L}_2^2(\partial D)$, $\mathbf{H}_2^s(\partial D)$ and $\mathbf{C}_2^{m,\sigma}(\partial D)$ are defined likewise.

Just like \mathbb{M} and \mathbb{J} , the operators \mathbb{M}^* , \mathbb{J}^* , $\mathbb{M}^*\mathbb{M}$, and $\mathbb{J}^*\mathbb{J}$ can be expressed as weakly singular integral operators; this is due to results in [22, Part I, Chapter 2, sections 1.1.2, 1.1.3]. It follows that these operators are also continuous and compact on $\mathbf{C}^m(\partial D) \times \mathbf{C}^m(\partial D)$ and on $\mathbf{H}^s(\partial D) \times \mathbf{H}^s(\partial D)$ provided that ∂D has at least regularity $C^{1,\sigma}$ with $\sigma > 0$.

We now state our all-frequency stable weakly-singular SIE system governed by an operator of the form $\mathbb{I} + \tilde{\mathbb{M}}$, where $\tilde{\mathbb{M}}$ is a self-adjoint operator that incorporates the stabilization operator intrinsically.

Theorem 2. *Let $[\mathbf{e}, \mathbf{h}]$ be the unique solution to equation (46). Then $[\mathbf{e}, \mathbf{h}]$ is also the unique solution to the equation*

$$\left[\mathbb{I} + \mathbb{M}^*\mathbb{M} + \mathbb{M} + \mathbb{M}^* + \mathbb{J}^*\mathbb{J} \right] \begin{pmatrix} \mathbf{e} \\ \mathbf{h} \end{pmatrix} = \left[\mathbb{I} + \mathbb{M}^* \right] \begin{pmatrix} \mathbf{f} \\ \mathbf{g} \end{pmatrix}. \quad (47)$$

The solution $(\mathbf{e}, \mathbf{h})^T$ depends continuously on $(\mathbf{f}, \mathbf{g})^T$ and this continuous dependence is valid in any space $\mathbf{C}_2^{m,\sigma}(\partial D)$ or $\mathbf{H}_2^s(\partial D)$ with $m \in \mathbb{N}$, $\sigma \in [0, 1]$, $s \geq 0$, provided that ∂D has sufficient regularity.

The proof of Theorem 2 first requires two general lemmas.

Lemma 3. *Let H be a Hilbert space and $\mathbb{M}, \mathbb{J} : H \rightarrow H$ two compact linear operators such that $N(\mathbb{J}) \cap N(\mathbb{I} + \mathbb{M}) = \{0\}$. Then the linear operator $\mathbb{I} + \mathbb{M}^*\mathbb{M} + \mathbb{M}^* + \mathbb{M} + \mathbb{J}^*\mathbb{J}$ has a bounded inverse.*

Proof. We note that $\mathbb{I} + \mathbb{M}^*\mathbb{M} + \mathbb{M}^* + \mathbb{M} = (\mathbb{I} + \mathbb{M})^*(\mathbb{I} + \mathbb{M})$. If $x \in H$ is such that $(\mathbb{I} + \mathbb{M})^*(\mathbb{I} + \mathbb{M})x + \mathbb{J}^*\mathbb{J}x = 0$, then $\|(\mathbb{I} + \mathbb{M})x\|^2 + \|\mathbb{J}x\|^2 = 0$, so $x \in N(\mathbb{J}) \cap N(\mathbb{I} + \mathbb{M})$. It follows that, due to our assumption, x must be zero. Since $\mathbb{M}^*\mathbb{M} + \mathbb{M}^* + \mathbb{M} + \mathbb{J}^*\mathbb{J}$ is compact, it follows that $\mathbb{I} + \mathbb{M}^*\mathbb{M} + \mathbb{M}^* + \mathbb{M} + \mathbb{J}^*\mathbb{J}$ has a bounded inverse. \square

Lemma 4. *Let $H, \mathbb{M}, \mathbb{J}$ be defined as in the previous lemma, with $N(\mathbb{J}) \cap N(\mathbb{I} + \mathbb{M}) = \{0\}$. Assume also that the system of equations*

$$\begin{cases} (\mathbb{I} + \mathbb{M})x = b \\ \mathbb{J}x = 0 \end{cases} \quad (48)$$

has a solution $x_0 \in H$. Then x_0 is the unique solution to the equation

$$(\mathbb{I} + \mathbb{M}^*\mathbb{M} + \mathbb{M}^* + \mathbb{M} + \mathbb{J}^*\mathbb{J})x = (\mathbb{I} + \mathbb{M}^*)b. \quad (49)$$

Proof. Uniqueness follows from Lemma 3. Since x_0 satisfies (48) it is clear that $(\mathbb{I} + \mathbb{M}^*)(\mathbb{I} + \mathbb{M})x_0 = (\mathbb{I} + \mathbb{M}^*)b$ and $\mathbb{J}^*\mathbb{J}x_0 = 0$. Thus x_0 satisfies (49). \square

Theorem 2 is now proved thanks to the previous lemma and Theorem 1. There remains an important question: do we have a control over the norm of the inverse operator $(\mathbb{I} + \mathbb{M}^*\mathbb{M} + \mathbb{M}^* + \mathbb{M} + \mathbb{J}^*\mathbb{J})^{-1}$? To address this question, we now show that the norm of this inverse operator can be estimated using the norms of \mathbb{M} and \mathbb{J} , a constant that measures "how well" $(\mathbb{I} + \mathbb{M})$ is invertible on the orthogonal of $N(\mathbb{I} + \mathbb{M})$, and another constant that measures "how positive" $\mathbb{J}^*\mathbb{J}$ is on $N(\mathbb{I} + \mathbb{M})$.

We first note that $\mathbb{I} + \mathbb{M}$ is bijective from $N(\mathbb{I} + \mathbb{M})^\perp$ to $R(\mathbb{I} + \mathbb{M})$, and that its inverse is bounded. Denote by P the orthogonal projection on $N(\mathbb{I} + \mathbb{M})$. There is a positive constant C_1 such that for all $x \in H$,

$$\|(\mathbb{I} - P)x\| \leq C_1 \|(\mathbb{I} + \mathbb{M})(\mathbb{I} - P)x\|. \quad (50)$$

Next we note that $N(\mathbb{I} + \mathbb{M})$ is finite dimensional. Using that $N(\mathbb{J}) \cap N(\mathbb{I} + \mathbb{M}) = \{0\}$, $\|\mathbb{J}\|$ achieves a strictly positive minimum on the compact set $\{x : x \in N(\mathbb{I} + \mathbb{M}), \|x\| = 1\}$. Therefore, there is a positive constant C_2 such that for all $x \in H$,

$$\|Px\| \leq C_2 \|\mathbb{J}Px\|. \quad (51)$$

Assume now that

$$(\mathbb{I} + \mathbb{M})^*(\mathbb{I} + \mathbb{M})x + \mathbb{J}^*\mathbb{J}x = d, \quad (52)$$

for some d , and estimate x .

There are two cases. Let us first consider the case when $d \in N(\mathbb{I} + \mathbb{M})^\perp$, that is, $d = (\mathbb{I} - P)d$. Evaluating the dot product of x with (52), we obtain

$$\|(\mathbb{I} + \mathbb{M})x\|^2 + \|\mathbb{J}x\|^2 = \langle x, (\mathbb{I} - P)d \rangle,$$

which we re-write as

$$\|(\mathbb{I} + \mathbb{M})(\mathbb{I} - P)x\|^2 + \|\mathbb{J}x\|^2 = \langle (\mathbb{I} - P)x, d \rangle.$$

Using (50),

$$\frac{1}{C_1^2} \|(\mathbb{I} - P)x\|^2 + \|\mathbb{J}x\|^2 \leq \|(\mathbb{I} - P)x\| \|d\|.$$

Thus, we obtain

$$\|(\mathbb{I} - P)x\| \leq C_1^2 \|d\|, \quad \|\mathbb{J}x\| \leq C_1 \|d\|. \quad (53)$$

It now follows that,

$$\|\mathbb{J}Px\| \leq \|\mathbb{J}x\| + \|\mathbb{J}(\mathbb{I} - P)x\| \leq (C_1 + C_1^2 \|\mathbb{J}\|) \|d\|,$$

and using (51),

$$\|Px\| \leq C_2 (C_1 + C_1^2 \|\mathbb{J}\|) \|d\|. \quad (54)$$

Thus, we obtain the bound

$$\|x\|^2 = \|Px\|^2 + \|(\mathbb{I} - P)x\|^2 \leq \left(C_2^2 (C_1 + C_1^2 \|\mathbb{J}\|)^2 + C_1^4 \right) \|d\|^2. \quad (55)$$

Let us now consider the case when $d \in N(\mathbb{I} + \mathbb{M})$ and estimate $\|x\|$ from (52). Using that $Pd = d$ and evaluating the inner product of equation (52) with x , we obtain,

$$\|(\mathbb{I} + \mathbb{M})(\mathbb{I} - P)x\|^2 + \|\mathbb{J}x\|^2 = \langle Px, d \rangle. \quad (56)$$

Next, we evaluate the inner product of equation (52) with Px to obtain

$$\langle \mathbb{J}Px, \mathbb{J}x \rangle = \langle Px, d \rangle. \quad (57)$$

Combining (56) with (57) we arrive at

$$\|(\mathbb{I} + \mathbb{M})(\mathbb{I} - P)x\|^2 + \frac{1}{2}\|\mathbb{J}x\|^2 \leq \frac{1}{2}\|\mathbb{J}Px\|^2. \quad (58)$$

From (56) and (50)

$$\|(\mathbb{I} - P)x\|^2 \leq C_1^2 \langle Px, d \rangle. \quad (59)$$

Next, we note that, using (57),

$$\|\mathbb{J}Px\|^2 = \langle Px, d \rangle - \langle \mathbb{J}Px, \mathbb{J}(\mathbb{I} - P)x \rangle \leq \langle Px, d \rangle + \frac{1}{2}\|\mathbb{J}Px\|^2 + \frac{1}{2}\|\mathbb{J}(\mathbb{I} - P)x\|^2,$$

so combining (59) and (60),

$$\frac{1}{2}\|\mathbb{J}Px\|^2 \leq \left(1 + \frac{1}{2}C_1^2 \|\mathbb{J}\|^2 \right) \langle Px, d \rangle, \quad (60)$$

and recalling (51),

$$\|Px\|^2 \leq C_2^2 (2 + C_1^2 \|\mathbb{J}\|^2) \langle Px, d \rangle \leq \frac{1}{2}\|Px\|^2 + \frac{1}{2}C_2^4 (2 + C_1^2 \|\mathbb{J}\|^2)^2 \|d\|^2,$$

thus

$$\|Px\|^2 \leq C_2^4 (2 + C_1^2 \|\mathbb{J}\|^2)^2 \|d\|^2. \quad (61)$$

Using (59) one more time, it follows that

$$\|(\mathbb{I} - P)x\|^2 \leq C_1^2 C_2^2 (2 + C_1^2 \|\mathbb{J}\|^2) \|d\|^2. \quad (62)$$

Combining (61) and (62), it is clear that $\|x\|$ is bounded by a constant depending only on C_1, C_2 , and $\|\mathbb{J}\| \|d\|$.

We covered two cases: if $d \in N(\mathbb{I} + \mathbb{M})^\perp$ then the estimate (55) holds, and if $d \in N(\mathbb{I} + \mathbb{M})$ then the estimate (61-62) holds. Since H is the direct sum of $N(\mathbb{I} + \mathbb{M})^\perp$ and $N(\mathbb{I} + \mathbb{M})$ and equation (52) is linear, the estimate for $d \in H$ results from combining the previous two estimates.

Remark 5. *In the trivial case where the nullspace of $\mathbb{I} + \mathbb{M}$ is reduced to zero, we have that $(\mathbb{I} - P) = \mathbb{I}$. Consequently, (53) reduces to $\|x\| \leq C_1^2 \|d\|$, that is, the norm of $(\mathbb{I} + \mathbb{M}^* \mathbb{M} + \mathbb{M}^* + \mathbb{M} + \mathbb{J}^* \mathbb{J})^{-1}$ is bounded by C_1^2 .*

Although it is clear that the operator $\mathbb{I} + \mathbb{M}^* \mathbb{M} + \mathbb{M}^* + \mathbb{M} + \mathbb{J}^* \mathbb{J}$ is bounded as ω tends to zero, we have yet to argue that its inverse too remains bounded in this limiting case. As mentioned in the introduction, this will prove that our integral equation formulation does not suffer from the well documented low frequency breakdown. We emphasize that this property holds for the continuous operators and thus any numerical method that correctly approximates these operators will inherit this no breakdown property. In this paragraph we temporarily mark the dependence of operators on the frequency ω explicitly.

Theorem 6. *For $\omega > 0$ the operator $\mathbb{I} + \mathbb{M}^*(\omega)\mathbb{M}(\omega) + \mathbb{M}^*(\omega) + \mathbb{M}(\omega) + \mathbb{J}^*(\omega)\mathbb{J}(\omega)$ acting on $\mathbf{C}_2^{m,\sigma}(\partial D)$ or on $\mathbf{H}_2^s(\partial D)$ depends continuously on ω . As ω tends to zero, it converges strongly to the operator $\mathbb{I} + \mathbb{M}^*(0)\mathbb{M}(0) + \mathbb{M}(0) + \mathbb{M}^*(0)$. Assuming that ϵ^\pm and μ^\pm are as specified in Section 1, this latter operator is invertible and its inverse is continuous. Accordingly, the inverse of $\mathbb{I} + \mathbb{M}^*(\omega)\mathbb{M}(\omega) + \mathbb{M}^*(\omega) + \mathbb{M}(\omega) + \mathbb{J}^*(\omega)\mathbb{J}(\omega)$ remains uniformly bounded as $\omega \rightarrow 0$.*

Proof. Denote

$$G_0(\mathbf{x}, \mathbf{y}) = \frac{1}{4\pi|\mathbf{x} - \mathbf{y}|}. \quad (63)$$

Write

$$\epsilon^+ \pm G_+(x, y) - \epsilon^- \pm G_-(x, y) - (\epsilon^+ - \epsilon^-)G_0(x, y) = \omega R(x, y) \quad (64)$$

where the remainder R is given by

$$R(x, y) = \sum_{l=1}^{\infty} \frac{1}{l!} \omega^{l-1} |x - y|^{l-1} i^l ((\mu^+ \epsilon^+)^{\frac{l}{2}} - (\mu^- \epsilon^-)^{\frac{l}{2}}). \quad (65)$$

Clearly, R is uniformly bounded on $\partial D \times \partial D$ for ω in $(0, 1)$. For $x \neq y$ in ∂D , $R(x, y)$ has infinitely many derivatives and there is an upper bound for the supremum of these derivatives that is independent of ω . It follows that the boundary integral operator associated to R is continuous on $\mathbf{C}_2^{m,\sigma}(\partial D)$ or on $\mathbf{H}_2^s(\partial D)$ and its norm is bounded above by a constant independent of ω in $(0, 1)$. Recall the definition of the operator $\underline{\mathcal{D}}_\pm$ introduced in (28) which is involved in (27) and hence further in the definition of $\tilde{\mathcal{C}}^{(\alpha^+, \alpha^-)}$ in (34). The argument above shows that the operator $\epsilon_+ \underline{\mathcal{D}}_+ - \epsilon_- \underline{\mathcal{D}}_-$ is

norm convergent as $\omega \rightarrow 0$ to the operator

$$\mathbf{w} \rightarrow (\epsilon_+ - \epsilon_-) \int_{\partial D} \frac{\partial G_0}{\partial \mathbf{n}(\mathbf{x})}(\mathbf{x}, \mathbf{y}) \mathbf{w}(\mathbf{y}) ds(\mathbf{y}). \quad (66)$$

This argument can be carried over to all the other operators involved in the definition of $\mathbb{M}(\omega)$ to show that it converges in operator norm to $\mathbb{M}(0)$ as $\omega \rightarrow 0$ and that $\mathbb{J}(\omega)$ converges in operator norm to zero. In [11, Appendix B] we gave an explicit formulation for $\mathbb{M}(0)$ and we proved that $\mathbb{I} + \mathbb{M}(0)$ has a bounded inverse. Altogether, we can claim that $\mathbb{I} + \mathbb{M}^*(\omega)\mathbb{M}(\omega) + \mathbb{M}^*(\omega) + \mathbb{M}(\omega) + \mathbb{J}^*(\omega)\mathbb{J}(\omega)$ is norm convergent to

$$\mathbb{I} + \mathbb{M}^*(0)\mathbb{M}(0) + \mathbb{M}^*(0) + \mathbb{M}(0) = (\mathbb{I} + \mathbb{M}(0))^*(\mathbb{I} + \mathbb{M}(0)). \quad (67)$$

Since this operator has a bounded inverse, the proof is complete. \square

Remark 7. In [11, Appendix B] no assumption was necessary on the genus of ∂D . The uniform well-posedness statement of Theorem 6 therefore holds regardless of the genus of ∂D .

5 Numerical algorithm and convergence analysis

For our numerical approach, we transform all of our integral operators to a reference surface S , the unit sphere. In particular, we use a bijective parametrization $\mathbf{q} : S \rightarrow \partial D$, which is not necessarily the standard spherical polar coordinates transformation, to transform the operators \mathbb{M} and \mathbb{J} to operators acting on spherical functions. To simplify notations, the resulting operators will still be denoted by \mathbb{J} and \mathbb{M} . Some smoothness is required of the transformation \mathbf{q} , which we describe in the final convergence theorem in this section. Note, however, that in atmospheric physics [26–28], the shapes of relevant particles satisfy this smoothness requirement.

5.1 Vector spherical polynomials

Our approximation to the surface fields on the reference surface using a finite dimensional space is based on the standard spherical harmonic basis $Y_{l,j}$, which is orthogonal with respect to the natural L^2 inner product (\cdot, \cdot) on the unit sphere S . In particular, to approximate the fields \mathbf{e} and \mathbf{h} in (47), we define $\mathbf{Y}_{l,j,k} = Y_{l,j}\mathbf{e}_k$, where \mathbf{e}_k for $k = 1, \dots, 3$ is the natural basis of \mathbb{C}^3 . Let \mathbb{P}_n be the span of $\mathbf{Y}_{l,j,k}$ for $0 \leq l \leq n$, $|j| \leq l$, $1 \leq k \leq 3$. As emphasized in [19], for discrete approximation of the inner product on S within the algorithm, it is essential to use a quadrature rule with m points $\hat{\mathbf{x}}_q^m$ and weights ζ_q^m for $q = 1, \dots, m$ that computes inner products between any two elements in \mathbb{P}_n exactly. Such a quadrature rule with $m = 2(n+1)^2$ can be found in [19].

In particular, if we denote by $(\cdot, \cdot)_m$ the bilinear product obtained by approximating the inner product (\cdot, \cdot) on $\mathbf{C}_2(S)$ using the points $\hat{\mathbf{x}}_q^m$ and weights ζ_q^m for $q = 1, \dots, m$,

then

$$(\mathbf{G}, \mathbf{H})_m = (\mathbf{G}, \mathbf{H}), \quad \forall \mathbf{G}, \mathbf{H} \in \mathbb{P}_n. \quad (68)$$

In line with [19, Page 34], we will denote by $\underline{\mathcal{L}}_n : \mathbf{C}_2(S) \rightarrow \mathbb{P}_n$ the vector-valued fully-discrete orthogonal projection obtained using the discrete inner product $(\cdot, \cdot)_m$.

The key ingredient in our algorithm is to split \mathbb{M} into operators with weakly singular kernels \mathbb{M}_1 and smooth kernels \mathbb{M}_2 respectively. Details of such a splitting are given in [15, Section 3]. Following details in [15, Section 4], for integer $n' \geq n + 2$ we approximate the singular part \mathbb{M}_1 and regular part \mathbb{M}_2 of \mathbb{M} by $\mathbb{M}_{1,n'}$ and $\mathbb{M}_{2,n'}$ respectively. We similarly approximate \mathbb{J} by $\mathbb{J}_{n'}$ (and note that \mathbb{J} is regular and so has no singular part).

Our fully discrete numerical algorithm to compute the parametrized approximation $\Phi_n = (\mathbf{e}_n \circ \mathbf{q}, \mathbf{h}_n \circ \mathbf{q})^T$ to the unique solution $\Phi = (\mathbf{e} \circ \mathbf{q}, \mathbf{h} \circ \mathbf{q})^T$, defined on $S \times S$, of the transformed single-equation (47) on S with right hand side $F = [\mathbb{I} + \mathbb{M}^*](\mathbf{f} \circ \mathbf{q}, \mathbf{g} \circ \mathbf{q})^T$ can be expressed using the orthogonal projection operator as

$$(\mathbb{I} + \underline{\mathcal{L}}_n \mathbb{M}_{1,n'}^* \underline{\mathcal{L}}_n \mathbb{M}_{1,n'} \underline{\mathcal{L}}_n + \underline{\mathcal{L}}_n \mathbb{M}_{1,n'}^* \underline{\mathcal{L}}_n + \underline{\mathcal{L}}_n \mathbb{M}_{2,n'} \underline{\mathcal{L}}_n + \underline{\mathcal{L}}_n \mathbb{J}_{n'}^* \underline{\mathcal{L}}_n \mathbb{J}_{n'} \underline{\mathcal{L}}_n) \Phi_n = \underline{\mathcal{L}}_n F. \quad (69)$$

We omit a detailed description of how to implement the algorithm, which follows closely the detailed descriptions in [15, 19]. In the rest of this section we focus on proving spectrally accurate convergence of Φ_n to Φ as $n \rightarrow \infty$ under certain smoothness assumptions on F , that are dictated by the smoothness of the surface.

To prove well-posedness of the fully-discrete system (69), we first establish convergence of the approximate surface integral operators in an appropriate norm. Denote by $\|\cdot\|$ the supremum norm on $\mathbf{C}_2(S)$. The corresponding induced norm on the space of continuous linear operators from $\mathbf{C}_2(S)$ to $\mathbf{C}_2(S)$ will also be denoted by $\|\cdot\|$. The following two estimates for the vector-valued fully discrete projection operator were derived in [19, Appendix A], using associated scalar counterpart results in [29]:

$$\|\psi - \underline{\mathcal{L}}_n \psi\| \leq C n^{1/2} \|\psi\|, \quad (70)$$

for $\psi \in C(S)$, where C is independent of n , and

$$\|\psi - \underline{\mathcal{L}}_n \psi\| \leq C n^{1/2-r-\alpha} \|\psi\|_{\mathbf{C}_2^{r,\alpha}}, \quad (71)$$

for $\psi \in \mathbf{C}_2^{r,\alpha}(S)$, where C is independent of n .

Theorem 8. *For any p in \mathbb{N} , there is a positive constant c_p independent of n and $n' \geq n - 2$ such that*

$$\|(\mathbb{M} - \mathbb{M}_{1,n'} - \mathbb{M}_{2,n'}) \mathbf{P}_n\| + \|(\mathbb{J} - \mathbb{J}_{n'}) \mathbf{P}_n\| \leq c_p n^{-p} \|\mathbf{P}_n\|, \quad (72)$$

for all \mathbf{P}_n in \mathbb{P}_n .

Proof. See [19]. □

To simplify the notation set $\mathbb{M}_{n'} = \mathbb{M}_{1,n'} + \mathbb{M}_{2,n'}$. Using (70), there is an interesting way to rewrite estimate (72) in terms of norm operators from $\mathbf{C}_2(S)$ to $\mathbf{C}_2(S)$,

$$\|(\mathbb{M} - \mathbb{M}_{n'})\underline{\mathcal{L}}_n\| + \|(\mathbb{J} - \mathbb{J}_{n'})\underline{\mathcal{L}}_n\| \leq c_p n^{1/2-p}. \quad (73)$$

The adjoint operators \mathbb{M}^* and \mathbb{J}^* can also be approximated as in [19] by $\mathbb{M}_{n'}^*$ and $\mathbb{J}_{n'}^*$, and the following estimate holds

$$\|(\mathbb{M}^* - \mathbb{M}_{n'}^*)\underline{\mathcal{L}}_n\| + \|(\mathbb{J}^* - \mathbb{J}_{n'}^*)\underline{\mathcal{L}}_n\| \leq c_p n^{1/2-p}. \quad (74)$$

Proving existence and uniqueness of the solution of the discrete analogue of $(\mathbb{I} + \mathbb{M}^*\mathbb{M} + \mathbb{M} + \mathbb{M}^* + \mathbb{J}^*\mathbb{J})\Phi = F$ in the space \mathbb{P}_n , and that the solution converges to Φ , is rather involved. The main hurdle is that the norm of the projection operator $\underline{\mathcal{L}}_n$ from $\mathbf{C}_2(S)$ to \mathbb{P}_n becomes unbounded as n grows large. In fact, it was shown in [29] that this norm is exactly of the order $n^{1/2}$ (for a scalar counterpart of $\underline{\mathcal{L}}_n$).

Lemma 9. *For all sufficiently large n , the linear operator*

$$\mathbb{I} + \mathbb{M}^*\underline{\mathcal{L}}_n\mathbb{M}\underline{\mathcal{L}}_n + \mathbb{M}^*\underline{\mathcal{L}}_n + \mathbb{M}\underline{\mathcal{L}}_n + \mathbb{J}^*\underline{\mathcal{L}}_n\mathbb{J}\underline{\mathcal{L}}_n : \mathbf{C}_2(S) \rightarrow \mathbf{C}_2(S)$$

is invertible. For all sufficiently large n ,

$$\begin{aligned} \|(\mathbb{I} + \mathbb{M}^*\underline{\mathcal{L}}_n\mathbb{M}\underline{\mathcal{L}}_n + \mathbb{M}^*\underline{\mathcal{L}}_n + \mathbb{M}\underline{\mathcal{L}}_n + \mathbb{J}^*\underline{\mathcal{L}}_n\mathbb{J}\underline{\mathcal{L}}_n)^{-1}\| &\leq Cn^{1/2}, \\ \|\mathbb{M}^*\underline{\mathcal{L}}_n\mathbb{M}\underline{\mathcal{L}}_n + \mathbb{M}^*\underline{\mathcal{L}}_n + \mathbb{M}\underline{\mathcal{L}}_n + \mathbb{J}^*\underline{\mathcal{L}}_n\mathbb{J}\underline{\mathcal{L}}_n\| &\leq Cn^{1/2}, \end{aligned}$$

where C is a constant.

Proof. Because $\mathbb{M}, \mathbb{J} : \mathbf{C}_2(S) \rightarrow \mathbf{C}_2^\alpha(S)$ are continuous operators for any α in $(0, 1)$ so in particular for α in $(\frac{1}{2}, 1)$, it follows from (71) that

$$\|(\mathbb{I} - \underline{\mathcal{L}}_n)\mathbb{M}\| + \|(\mathbb{I} - \underline{\mathcal{L}}_n)\mathbb{J}\| + \|(\mathbb{I} - \underline{\mathcal{L}}_n)\mathbb{M}^*\| \rightarrow 0, \quad \text{as } n \rightarrow \infty,$$

so

$$\|\mathbb{M}^*(\mathbb{I} - \underline{\mathcal{L}}_n)\mathbb{M} + (\mathbb{I} - \underline{\mathcal{L}}_n)\mathbb{M}^* + (\mathbb{I} - \underline{\mathcal{L}}_n)\mathbb{M} + \mathbb{J}^*(\mathbb{I} - \underline{\mathcal{L}}_n)\mathbb{J}\| \rightarrow 0, \quad \text{as } n \rightarrow \infty.$$

Then using that $\mathbb{I} + \mathbb{M}^*\mathbb{M} + \mathbb{M} + \mathbb{M}^* + \mathbb{J}^*\mathbb{J}$ is invertible, it follows that $\mathbb{I} + \mathbb{M}^*\underline{\mathcal{L}}_n\mathbb{M} + \underline{\mathcal{L}}_n\mathbb{M}^* + \underline{\mathcal{L}}_n\mathbb{M} + \mathbb{J}^*\underline{\mathcal{L}}_n\mathbb{J}$ is invertible with $n > N$ for some N , and $\|(\mathbb{I} + \mathbb{M}^*\underline{\mathcal{L}}_n\mathbb{M} + \underline{\mathcal{L}}_n\mathbb{M}^* + \underline{\mathcal{L}}_n\mathbb{M} + \mathbb{J}^*\underline{\mathcal{L}}_n\mathbb{J})^{-1}\|$ is uniformly bounded for $n > N$ and convergent to $\|(\mathbb{I} + \mathbb{M}^*\mathbb{M} + \mathbb{M}^* + \mathbb{M} + \mathbb{J}^*\mathbb{J})^{-1}\|$. Let Φ be in $\mathbf{C}_2(S)$ and fix $\alpha \in (1/2, 1)$. Then using (71),

$$\begin{aligned} \|(\mathbb{I} - \underline{\mathcal{L}}_n)\mathbb{M}^*\underline{\mathcal{L}}_n\mathbb{M}\Phi\| &\leq Cn^{1/2-\alpha}\|\mathbb{M}^*\underline{\mathcal{L}}_n\mathbb{M}\Phi\|_{\mathbf{C}_2^\alpha} \\ &\leq Cn^{1/2-\alpha}\|\underline{\mathcal{L}}_n\mathbb{M}\Phi\| \\ &\leq Cn^{1/2-\alpha}\|(\mathbb{I} - \underline{\mathcal{L}}_n)\mathbb{M}\Phi\| + Cn^{1/2-\alpha}\|\mathbb{M}\Phi\| \\ &\leq Cn^{1-2\alpha}\|\mathbb{M}\Phi\|_{\mathbf{C}^\alpha} + Cn^{1/2-\alpha}\|\mathbb{M}\Phi\| \\ &\leq Cn^{1-2\alpha}\|\Phi\| + Cn^{1/2-\alpha}\|\Phi\|. \end{aligned}$$

Thus $\|(\mathbb{I} - \underline{\mathcal{L}}_n)\mathbb{M}^*\underline{\mathcal{L}}_n\mathbb{M}\| \rightarrow 0$ as $n \rightarrow \infty$. A similar result holds for $\|(\mathbb{I} - \underline{\mathcal{L}}_n)\mathbb{J}^*\underline{\mathcal{L}}_n\mathbb{J}\|$. It follows that $\mathbb{I} + \underline{\mathcal{L}}_n\mathbb{M}^*\underline{\mathcal{L}}_n\mathbb{M} + \underline{\mathcal{L}}_n\mathbb{M}^* + \underline{\mathcal{L}}_n\mathbb{M} + \underline{\mathcal{L}}_n\mathbb{J}^*\underline{\mathcal{L}}_n\mathbb{J}$ is invertible for $n \geq N_2$ for some N_2 , and $\|(\mathbb{I} + \underline{\mathcal{L}}_n\mathbb{M}^*\underline{\mathcal{L}}_n\mathbb{M} + \underline{\mathcal{L}}_n\mathbb{M}^* + \underline{\mathcal{L}}_n\mathbb{M} + \underline{\mathcal{L}}_n\mathbb{J}^*\underline{\mathcal{L}}_n\mathbb{J})^{-1}\|$ is uniformly bounded for $n > N_2$ and convergent to $\|(\mathbb{I} + \mathbb{M}^*\mathbb{M} + \mathbb{M}^* + \mathbb{M} + \mathbb{J}^*\mathbb{J})^{-1}\|$.

A simple calculation using the identity

$$(I + BA)(I - B(I + AB)^{-1}A) = (I - B(I + AB)^{-1}A)(I + BA) = I$$

shows that the inverse of $\mathbb{I} + \mathbb{M}^*\underline{\mathcal{L}}_n\mathbb{M}\underline{\mathcal{L}}_n + \mathbb{M}^*\underline{\mathcal{L}}_n + \mathbb{M}\underline{\mathcal{L}}_n + \mathbb{J}^*\underline{\mathcal{L}}_n\mathbb{J}\underline{\mathcal{L}}_n$ is

$$\mathbb{I} - (\mathbb{M}^*\underline{\mathcal{L}}_n\mathbb{M} + \mathbb{M}^* + \mathbb{M} + \mathbb{J}^*\underline{\mathcal{L}}_n\mathbb{J})(\mathbb{I} + \underline{\mathcal{L}}_n\mathbb{M}^*\underline{\mathcal{L}}_n\mathbb{M} + \underline{\mathcal{L}}_n\mathbb{M}^* + \underline{\mathcal{L}}_n\mathbb{M} + \underline{\mathcal{L}}_n\mathbb{J}^*\underline{\mathcal{L}}_n\mathbb{J})^{-1}\underline{\mathcal{L}}_n.$$

At this stage we recall that $\|(\mathbb{I} + \underline{\mathcal{L}}_n\mathbb{M}^*\underline{\mathcal{L}}_n\mathbb{M} + \underline{\mathcal{L}}_n\mathbb{M}^* + \underline{\mathcal{L}}_n\mathbb{M} + \underline{\mathcal{L}}_n\mathbb{J}^*\underline{\mathcal{L}}_n\mathbb{J})^{-1}\|$ and $\|\mathbb{M}^*\underline{\mathcal{L}}_n\mathbb{M} + \mathbb{M}^* + \mathbb{M} + \mathbb{J}^*\underline{\mathcal{L}}_n\mathbb{J}\|$ are bounded, and that $\|\underline{\mathcal{L}}_n\| \leq Cn^{1/2}$ to conclude that

$$\|(\mathbb{I} + \mathbb{M}^*\underline{\mathcal{L}}_n\mathbb{M}\underline{\mathcal{L}}_n + \mathbb{M}^*\underline{\mathcal{L}}_n + \mathbb{M}\underline{\mathcal{L}}_n + \mathbb{J}^*\underline{\mathcal{L}}_n\mathbb{J}\underline{\mathcal{L}}_n)^{-1}\| \leq Cn^{1/2}. \quad (75)$$

Similar arguments show that $\|\mathbb{M}^*\underline{\mathcal{L}}_n\mathbb{M}\underline{\mathcal{L}}_n + \mathbb{M}^*\underline{\mathcal{L}}_n + \mathbb{M}\underline{\mathcal{L}}_n + \mathbb{J}^*\underline{\mathcal{L}}_n\mathbb{J}\underline{\mathcal{L}}_n\| \leq Cn^{1/2}$. \square

Theorem 10. *The linear operator*

$$\mathbb{I} + \underline{\mathcal{L}}_n\mathbb{M}_{n'}^*\underline{\mathcal{L}}_n\mathbb{M}_{n'}\underline{\mathcal{L}}_n + \underline{\mathcal{L}}_n\mathbb{M}_{n'}^*\underline{\mathcal{L}}_n + \underline{\mathcal{L}}_n\mathbb{M}_{n'}\underline{\mathcal{L}}_n + \underline{\mathcal{L}}_n\mathbb{J}_{n'}^*\underline{\mathcal{L}}_n\mathbb{J}_{n'}\underline{\mathcal{L}}_n : \underline{\mathbb{P}}_n \rightarrow \underline{\mathbb{P}}_n$$

is invertible for all sufficiently large n and $n' \geq n + 2$. Additionally, if $\Phi \in C(S)$ is the unique solution to

$$(\mathbb{I} + \mathbb{M}^*\mathbb{M} + \mathbb{M}^* + \mathbb{M} + \mathbb{J}^*\mathbb{J})\Phi = F, \quad (76)$$

where, for $r > 2$ (depending on the smoothness of the parametrization map \mathbf{q}), F is in $C^{r,\alpha}(S)$ with $\alpha \in (1/2, 1)$, and if for sufficiently large n , $\Phi_n \in \underline{\mathbb{P}}_n$ solves

$$(\mathbb{I} + \underline{\mathcal{L}}_n\mathbb{M}_{n'}^*\underline{\mathcal{L}}_n\mathbb{M}_{n'}\underline{\mathcal{L}}_n + \underline{\mathcal{L}}_n\mathbb{M}_{n'}^*\underline{\mathcal{L}}_n + \underline{\mathcal{L}}_n\mathbb{M}_{n'}\underline{\mathcal{L}}_n + \underline{\mathcal{L}}_n\mathbb{J}_{n'}^*\underline{\mathcal{L}}_n\mathbb{J}_{n'}\underline{\mathcal{L}}_n)\Phi_n = \underline{\mathcal{L}}_n F, \quad (77)$$

then there is a constant C independent of n and $n' \geq n + 2$ such that

$$\|\Phi - \Phi_n\| \leq Cn^{5/2-r-\alpha}\|F\|_{C_2^{r,\alpha}}. \quad (78)$$

Proof. From (70), we note that $\underline{\mathcal{L}}_n : \mathbf{C}_2(S) \rightarrow \mathbf{C}_2(S)$ is a bounded linear operator and

$$\|\underline{\mathcal{L}}_n\| \leq Cn^{1/2}. \quad (79)$$

Combining this with (73), establishes

$$\|\underline{\mathcal{L}}_n(\mathbb{M} - \mathbb{M}_{n'})\underline{\mathcal{L}}_n\| \leq Cn^{1-p},$$

where C depends on p . Then

$$\|\mathbb{M}^* \underline{\mathcal{L}}_n (\mathbb{M} - \mathbb{M}_{n'}) \underline{\mathcal{L}}_n\| \leq Cn^{1-p}, \quad (80)$$

and, combining (73) with (74),

$$\|(\mathbb{M}^* - \mathbb{M}_{n'}^*) \underline{\mathcal{L}}_n (\mathbb{M} - \mathbb{M}_{n'}) \underline{\mathcal{L}}_n\| \leq Cn^{1-p}. \quad (81)$$

Combining (80) and (81) yields

$$\|(\mathbb{M}^* + \mathbb{M}_{n'}^*) \underline{\mathcal{L}}_n (\mathbb{M} - \mathbb{M}_{n'}) \underline{\mathcal{L}}_n\| \leq Cn^{1-p}. \quad (82)$$

Next, we write

$$\begin{aligned} & \mathbb{M}_{n'}^* \underline{\mathcal{L}}_n \mathbb{M} \underline{\mathcal{L}}_n - \mathbb{M}^* \underline{\mathcal{L}}_n \mathbb{M}_{n'} \underline{\mathcal{L}}_n \\ &= (\mathbb{M}_{n'}^* - \mathbb{M}^*) \underline{\mathcal{L}}_n \mathbb{M} \underline{\mathcal{L}}_n - \mathbb{M}^* \underline{\mathcal{L}}_n (\mathbb{M}_{n'} - \mathbb{M}) \underline{\mathcal{L}}_n, \end{aligned}$$

so, by another application of (73)–(74) and (79) we have

$$\|\mathbb{M}_{n'}^* \underline{\mathcal{L}}_n \mathbb{M} \underline{\mathcal{L}}_n - \mathbb{M}^* \underline{\mathcal{L}}_n \mathbb{M}_{n'} \underline{\mathcal{L}}_n\| \leq Cn^{1-p}. \quad (83)$$

We now combine (82) with (83) to obtain

$$\|\mathbb{M}^* \underline{\mathcal{L}}_n \mathbb{M} \underline{\mathcal{L}}_n - \mathbb{M}_{n'}^* \underline{\mathcal{L}}_n \mathbb{M}_{n'} \underline{\mathcal{L}}_n\| \leq Cn^{1-p}. \quad (84)$$

Similarly,

$$\|\mathbb{J}^* \underline{\mathcal{L}}_n \mathbb{J} \underline{\mathcal{L}}_n - \mathbb{J}_{n'}^* \underline{\mathcal{L}}_n \mathbb{J}_{n'} \underline{\mathcal{L}}_n\| \leq Cn^{1-p}. \quad (85)$$

Finally, choosing $p > 3/2$ and recalling (73)–(74) we conclude using Lemma 9 that $\mathbb{I} + \mathbb{M}_{n'}^* \underline{\mathcal{L}}_n \mathbb{M}_{n'} \underline{\mathcal{L}}_n + \mathbb{M}_{n'}^* \underline{\mathcal{L}}_n + \mathbb{M}_{n'} \underline{\mathcal{L}}_n + \mathbb{J}_{n'}^* \underline{\mathcal{L}}_n \mathbb{J}_{n'} \underline{\mathcal{L}}_n$ is invertible for sufficiently large n and for those n thereupon,

$$\|(\mathbb{I} + \mathbb{M}_{n'}^* \underline{\mathcal{L}}_n \mathbb{M}_{n'} \underline{\mathcal{L}}_n + \mathbb{M}_{n'}^* \underline{\mathcal{L}}_n + \mathbb{M}_{n'} \underline{\mathcal{L}}_n + \mathbb{J}_{n'}^* \underline{\mathcal{L}}_n \mathbb{J}_{n'} \underline{\mathcal{L}}_n)^{-1}\| \leq Cn^{1/2}. \quad (86)$$

Now let $F \in \mathbf{C}_2(S)$, and Ψ_n solve

$$(\mathbb{I} + \mathbb{M}_{n'}^* \underline{\mathcal{L}}_n \mathbb{M}_{n'} \underline{\mathcal{L}}_n + \mathbb{M}_{n'}^* \underline{\mathcal{L}}_n + \mathbb{M}_{n'} \underline{\mathcal{L}}_n + \mathbb{J}_{n'}^* \underline{\mathcal{L}}_n \mathbb{J}_{n'} \underline{\mathcal{L}}_n) \Psi_n = \underline{\mathcal{L}}_n F. \quad (87)$$

As $(\underline{\mathcal{L}}_n)^2 = \underline{\mathcal{L}}_n$, left-multiplying equation (87) by $\underline{\mathcal{L}}_n$ shows that $\underline{\mathcal{L}}_n \Psi_n$ is the solution to

$$(\mathbb{I} + \underline{\mathcal{L}}_n \mathbb{M}_{n'}^* \underline{\mathcal{L}}_n \mathbb{M}_{n'} \underline{\mathcal{L}}_n + \underline{\mathcal{L}}_n \mathbb{M}_{n'}^* \underline{\mathcal{L}}_n + \underline{\mathcal{L}}_n \mathbb{M}_{n'} \underline{\mathcal{L}}_n + \underline{\mathcal{L}}_n \mathbb{J}_{n'}^* \underline{\mathcal{L}}_n \mathbb{J}_{n'} \underline{\mathcal{L}}_n) \Phi_n = \underline{\mathcal{L}}_n F. \quad (88)$$

We conclude that equation (77) is always solvable, and the solution is unique because $\underline{\mathbb{P}}_n$ is finite dimensional.

To prove estimate (78), let Φ_n be the unique solution to (77). According to the argument above, there is a unique $\Psi_n \in \mathbf{C}_2(S)$ such that $\Phi_n = \underline{\mathcal{L}}_n \Psi_n$ and Ψ_n is the unique solution to (87). Now define $\tilde{\Psi}_n$ to be the solution of

$$(\mathbb{I} + \mathbb{M}^* \mathbb{M} + \mathbb{M}^* + \mathbb{M} + \mathbb{J}^* \mathbb{J}) \tilde{\Psi}_n = \underline{\mathcal{L}}_n F. \quad (89)$$

As a byproduct of Theorem 2, we have that $\tilde{\Psi}_n \in \mathbf{C}_2^{r,\alpha}$ and

$$\|\tilde{\Psi}_n\|_{\mathbf{C}^{r,\alpha}} \leq C \|\underline{\mathcal{L}}_n F\|_{\mathbf{C}_2^{r,\alpha}}. \quad (90)$$

Now, using (71) and (73),

$$\begin{aligned} \|(\mathbb{M}_{n'} \underline{\mathcal{L}}_n - \mathbb{M}) \tilde{\Psi}_n\| &\leq \|\mathbb{M}(I - \underline{\mathcal{L}}_n) \tilde{\Psi}_n\| + \|(\mathbb{M}_{n'} - \mathbb{M}) \underline{\mathcal{L}}_n \tilde{\Psi}_n\| \\ &\leq C n^{1/2-r-\alpha} \|\tilde{\Psi}_n\|_{\mathbf{C}_2^{r,\alpha}}. \end{aligned} \quad (91)$$

Thus,

$$\|(\underline{\mathcal{L}}_n \mathbb{M}_{n'} \underline{\mathcal{L}}_n - \underline{\mathcal{L}}_n \mathbb{M}) \tilde{\Psi}_n\| \leq C n^{1-r-\alpha} \|\tilde{\Psi}_n\|_{\mathbf{C}_2^{r,\alpha}},$$

and as $\|(\mathbb{I} - \underline{\mathcal{L}}_n) \mathbb{M} \tilde{\Psi}_n\| \leq C n^{1/2-r-\alpha} \|\tilde{\Psi}_n\|_{\mathbf{C}_2^{r,\alpha}}$, we conclude that

$$\|(\underline{\mathcal{L}}_n \mathbb{M}_{n'} \underline{\mathcal{L}}_n - \mathbb{M}) \tilde{\Psi}_n\| \leq C n^{1-r-\alpha} \|\tilde{\Psi}_n\|_{\mathbf{C}_2^{r,\alpha}}. \quad (92)$$

Similarly,

$$\|(\underline{\mathcal{L}}_n \mathbb{M}_{n'}^* \underline{\mathcal{L}}_n - \mathbb{M}^*) \tilde{\Psi}_n\| \leq C n^{1-r-\alpha} \|\tilde{\Psi}_n\|_{\mathbf{C}_2^{r,\alpha}}. \quad (93)$$

From (91),

$$\|\mathbb{M}^*(\mathbb{M}_{n'} \underline{\mathcal{L}}_n - \mathbb{M}) \tilde{\Psi}_n\|_{\mathbf{C}_2^\alpha} \leq C n^{1/2-r-\alpha} \|\tilde{\Psi}_n\|_{\mathbf{C}_2^{r,\alpha}}, \quad (94)$$

and

$$\begin{aligned} \|\mathbb{M}^*(I - \underline{\mathcal{L}}_n)(\mathbb{M}_{n'} \underline{\mathcal{L}}_n - \mathbb{M}) \tilde{\Psi}_n\| &\leq C n^{1-r-\alpha} \|\tilde{\Psi}_n\|_{\mathbf{C}_2^{r,\alpha}}, \\ \|(\mathbb{M}_{n'}^* - \mathbb{M}^*) \underline{\mathcal{L}}_n (\mathbb{M}_{n'} \underline{\mathcal{L}}_n - \mathbb{M}) \tilde{\Psi}_n\|_\infty &\leq C n^{1-r-\alpha} \|\tilde{\Psi}_n\|_{\mathbf{C}_2^{r,\alpha}}, \end{aligned}$$

where in the last line we used (73). Thus, using (74),

$$\|(\mathbb{M}_{n'}^* \underline{\mathcal{L}}_n - \mathbb{M}^*)(\mathbb{M}_{n'} \underline{\mathcal{L}}_n - \mathbb{M}) \tilde{\Psi}_n\| \leq C n^{1-r-\alpha} \|\tilde{\Psi}_n\|_{\mathbf{C}_2^{r,\alpha}}. \quad (95)$$

Now combining (94) with (95) yields

$$\|(\mathbb{M}_{n'}^* \underline{\mathcal{L}}_n + \mathbb{M}^*)(\mathbb{M}_{n'} \underline{\mathcal{L}}_n - \mathbb{M}) \tilde{\Psi}_n\| \leq C n^{1-r-\alpha} \|\tilde{\Psi}_n\|_{\mathbf{C}_2^{r,\alpha}}. \quad (96)$$

To evaluate $(\mathbb{M}^* \mathbb{M}_{n'} \underline{\mathcal{L}}_n - \mathbb{M}_{n'}^* \underline{\mathcal{L}}_n \mathbb{M}) \tilde{\Psi}_n$, write

$$\begin{aligned} \|(\mathbb{M}^* \mathbb{M}_{n'} \underline{\mathcal{L}}_n - \mathbb{M}_{n'}^* \underline{\mathcal{L}}_n \mathbb{M}) \tilde{\Psi}_n\| &\leq \| \mathbb{M}^* (\mathbb{M}_{n'} - \mathbb{M}) \underline{\mathcal{L}}_n \tilde{\Psi}_n \| + \| \mathbb{M}^* (I - \underline{\mathcal{L}}_n) \mathbb{M} \underline{\mathcal{L}}_n \tilde{\Psi}_n \| \\ &\quad + \| \mathbb{M}^* \underline{\mathcal{L}}_n \mathbb{M} (-I + \underline{\mathcal{L}}_n) \tilde{\Psi}_n \| + \| (\mathbb{M}^* - \mathbb{M}_{n'}^*) \underline{\mathcal{L}}_n \mathbb{M} \tilde{\Psi}_n \| \end{aligned} \quad (97)$$

The first, third and fourth terms in the right hand side of (97) are clearly bounded by $Cn^{1-r-\alpha} \|\tilde{\Psi}_n\|_{\mathbf{C}_2^{r,\alpha}}$. To tackle the second term in (97), we write

$$\| \mathbb{M}^* (I - \underline{\mathcal{L}}_n) \mathbb{M} \underline{\mathcal{L}}_n \tilde{\Psi}_n \| \leq \| \mathbb{M}^* (I - \underline{\mathcal{L}}_n) \mathbb{M} \tilde{\Psi}_n \| + \| \mathbb{M}^* (I - \underline{\mathcal{L}}_n) \mathbb{M} (\mathbb{I} - \underline{\mathcal{L}}_n) \tilde{\Psi}_n \|,$$

which is again bounded by $Cn^{1-r-\alpha} \|\tilde{\Psi}_n\|$. Combining (96) with (97) it follows that

$$\|(\mathbb{M}_{n'}^* \underline{\mathcal{L}}_n \mathbb{M}_{n'} \underline{\mathcal{L}}_n - \mathbb{M}^* \mathbb{M}) \tilde{\Psi}_n\| \leq Cn^{1-r-\alpha} \|\tilde{\Psi}_n\|_{\mathbf{C}_2^{r,\alpha}}. \quad (98)$$

Similarly, we can show

$$\|(\mathbb{J}_{n'}^* \underline{\mathcal{L}}_n \mathbb{J}_{n'} \underline{\mathcal{L}}_n - \mathbb{J}^* \mathbb{J}) \tilde{\Psi}_n\| \leq Cn^{1-r-\alpha} \|\tilde{\Psi}_n\|_{\mathbf{C}_2^{r,\alpha}}. \quad (99)$$

Recalling that Ψ_n satisfies (87) and that $\tilde{\Psi}_n$ satisfies (89), it follows that (using (92), (93), (98), (99))

$$\begin{aligned} \|(\mathbb{I} + \mathbb{M}_{n'}^* \underline{\mathcal{L}}_n \mathbb{M}_{n'} \underline{\mathcal{L}}_n + \mathbb{M}_{n'}^* \underline{\mathcal{L}}_n + \mathbb{M}_{n'} \underline{\mathcal{L}}_n + \mathbb{J}_{n'}^* \underline{\mathcal{L}}_n \mathbb{J}_{n'} \underline{\mathcal{L}}_n) (\Psi_n - \tilde{\Psi}_n)\| \\ \leq Cn^{1-r-\alpha} \|\tilde{\Psi}_n\|_{\mathbf{C}_2^{r,\alpha}}. \end{aligned}$$

Now, using (86) we obtain

$$\|\Psi_n - \tilde{\Psi}_n\| \leq Cn^{3/2-r-\alpha} \|\tilde{\Psi}_n\|_{\mathbf{C}_2^{r,\alpha}}.$$

It follows from equations (76) and (89) that

$$\|\Phi - \tilde{\Psi}_n\| \leq C \|(\mathbb{I} - \underline{\mathcal{L}}_n) F\| \leq Cn^{1/2-r-\alpha} \|F\|_{\mathbf{C}_2^{r,\alpha}}.$$

It then follows from estimate (90) that

$$\|\Psi_n - \Phi\| \leq Cn^{2-r-\alpha} \|F\|_{\mathbf{C}_2^{r,\alpha}}. \quad (100)$$

Finally we recall that $\Phi_n = \underline{\mathcal{L}}_n \Psi_n$ and we use (100) and (70) to write

$$\|\Phi_n - \Phi\| \leq \|\underline{\mathcal{L}}_n \Psi_n - \underline{\mathcal{L}}_n \Phi\| + \|(\mathbb{I} - \underline{\mathcal{L}}_n) \Phi\| \leq Cn^{5/2-r-\alpha} \|F\|_{\mathbf{C}_2^{r,\alpha}},$$

so (78) is proved. \square

6 Numerical experiments

To demonstrate our algorithm we make use of a discretization that preserves adjointness. To that end, following details in [15] we write the component integral operators of \mathbb{M} and \mathbb{J} , defined in (35) and (43) respectively, in the form

$$\mathbf{f}(\mathbf{x}) = \int_{\partial D} m(\mathbf{x}, \mathbf{y}) \mathbf{w}(\mathbf{y}) ds(\mathbf{y}), \quad (101)$$

where the kernel $m(\mathbf{x}, \mathbf{y})$ is a 3×3 matrix and $\mathbf{w}(\mathbf{y})$, $\mathbf{f}(\mathbf{x})$ are column 3-vectors. As discussed earlier, we assume that the surface ∂D can be parametrized by a diffeomorphic map $\mathbf{q} : S \rightarrow \partial D$,

$$\mathbf{x} = \mathbf{q}(\hat{\mathbf{x}}), \quad \mathbf{x} \in \partial D, \quad \hat{\mathbf{x}} \in S. \quad (102)$$

Our discretization of (101) uses the transform back to the unit sphere S ,

$$\mathbf{F}(\hat{\mathbf{x}}) = \int_S M(\hat{\mathbf{x}}, \hat{\mathbf{y}}) \mathbf{W}(\hat{\mathbf{y}}) J(\hat{\mathbf{y}}) ds(\hat{\mathbf{y}}), \quad (103)$$

where J is the Jacobian of \mathbf{q} and

$$\begin{aligned} M(\hat{\mathbf{x}}, \hat{\mathbf{y}}) &= J(\hat{\mathbf{x}})^{1/2} m(\mathbf{q}(\hat{\mathbf{x}}), \mathbf{q}(\hat{\mathbf{y}})) J(\hat{\mathbf{y}})^{1/2}, \\ \mathbf{W}(\hat{\mathbf{x}}) &= J(\hat{\mathbf{x}})^{1/2} \mathbf{w}(\mathbf{q}(\hat{\mathbf{x}})), \\ \mathbf{F}(\hat{\mathbf{x}}) &= J(\hat{\mathbf{x}})^{1/2} \mathbf{f}(\mathbf{q}(\hat{\mathbf{x}})). \end{aligned} \quad (104)$$

The far-field \mathbf{E}_∞ is obtained similarly using surface integral representations [15, Section 3]. More precisely, we use Φ_n and the exact surface integral representation of the electric far-field \mathbf{E}^∞ in [11, Equation (6.2)] to compute the spectrally accurate approximation \mathbf{E}_n^∞ . Since the far-field kernels are smooth, following arguments in the final part of the proof in [19, Theorem 3], \mathbf{E}_n^∞ retains the same convergence properties with respect to n as Φ_n . The discretization described in Section 5, which uses a basis of spherical harmonics defined on the spherical reference domain S , then preserves adjointness of the transformed surface integral operators, so that the matrices representing \mathbb{M}^* and \mathbb{J}^* are readily computed as the conjugate transpose of the matrices representing \mathbb{M} and \mathbb{J} . In the remainder of this section we use the subscript n to denote approximations computed using the fully-discrete Galerkin scheme with spherical harmonics of degree not greater than n . Thus, for example, \mathbf{E}_n^∞ is our approximation to \mathbf{E}^∞ .

To demonstrate our algorithm we present numerical results for scattering of a plane wave

$$\mathbf{E}_{\text{inc}}(\mathbf{x}) = \mathbf{p} e^{ik \mathbf{x} \cdot \mathbf{d}}, \quad (105)$$

by a sphere, spheroids and a non-convex Chebyshev particle, which are common test geometries in the literature [26–28] and of interest in applications such as atmospheric science. (The sphere case facilitates comparison with the analytical Mie series solution [30].) Here \mathbf{d} is the incident wave direction, and \mathbf{p} satisfying $\mathbf{d} \cdot \mathbf{p} = 0$ is the

incident polarization. The spheroid with aspect ratio ρ is parametrized by

$$\mathbf{q}(\widehat{\mathbf{x}}) = \begin{pmatrix} \widehat{\mathbf{x}}_1/\rho \\ \widehat{\mathbf{x}}_2/\rho \\ \widehat{\mathbf{x}}_3 \end{pmatrix}, \quad \widehat{\mathbf{x}} \in S, \quad (106)$$

and is oriented so that its major axis aligns with the z -axis. The Chebyshev particle is parametrized by [28]

$$\mathbf{q}(\widehat{\mathbf{x}}) = r(\widehat{\mathbf{x}}) \widehat{\mathbf{x}}, \quad r(\widehat{\mathbf{x}}) = \frac{1}{2} + \frac{1}{40} \cos(5 \cos^{-1} \widehat{\mathbf{x}}_3). \quad \widehat{\mathbf{x}} \in S, \quad (107)$$

This particle is visualized in Figure 8. In our experiments we use dielectric bodies with real refractive index $\nu = 1.584$, which is the refractive index of polycarbonate, and based on numerical results in [26], absorbing bodies with complex refractive indices $\nu = 1.5 + 0.02i$, $1.0925 + 0.248i$. Thus we demonstrate our algorithm for non-absorbing, weakly-absorbing and strongly-absorbing particles. The electromagnetic size of the particles is $s = d/\lambda$ where d denotes the diameter of the particle, and the commonly used size parameter is therefore $x = \pi s$.

To simplify the exposition, except where otherwise stated, we compute the near field \mathbf{E} and the far field \mathbf{E}_n^∞ in the xz -plane for incident waves with direction $\mathbf{d} = (0, 0, 1)^T$. Thus the scattering plane is the xz -plane and, following [4, Page 245], [2, Page 387], and [3, Figure 4.5, Page 204] we define V-polarization and H-polarization as being respectively perpendicular and parallel to the scattering plane. In particular, for a receiver in the xz -plane in the direction $\widehat{\mathbf{x}} = (\sin \theta, 0, \cos \theta)^T$, we define the vertical and horizontal polarization directions respectively to be $\mathbf{e}_V = \mathbf{e}_\phi = (0, 1, 0)^T$ and $\mathbf{e}_H = \mathbf{e}_\theta = (\cos \theta, 0, -\sin \theta)^T$. The radar cross section of the scatterer, measured in the scattering plane, is then

$$\sigma_{XX}(\theta) = 10 \log_{10} 4\pi |\mathbf{e}_X(\theta) \cdot \mathbf{E}_\infty(\theta)|^2, \quad (108)$$

where $X = H$ or $X = V$ denotes the receiver polarization, and the incident wave polarization is chosen (H or V) to match the receiver polarization. The scattering plane and polarization are visualized in Figure 1.

In corroboration of the robust mathematical analysis in Section 4 proving all-frequency stability and well-posedness of the continuous system, we begin by numerically demonstrating the effectiveness of the fully-discrete counterpart of our new formulation (47), governed by second-kind self-adjoint operator $I + \widetilde{\mathbb{M}}$, compared with the related system (42), governed by $I + \mathbb{M}$ (both without further external constraints). To this end, in Figure 2 we plot the 1-norm condition number of the matrices representing both operators (obtained using the fully-discrete representation described above) for a unit sphere dielectric scatterer with refractive index $\nu = 1.303324617806156$, (for which $I + \mathbb{M}$ has an eigenfrequency $\omega = 4.638138138138138$). The plot was obtained using 1000 frequencies ω , which involves solving the Maxwell equations (4) more than 1000 times (with fixed dielectric constants and varying incident wave frequencies). The condition number is estimated in both cases using [31].

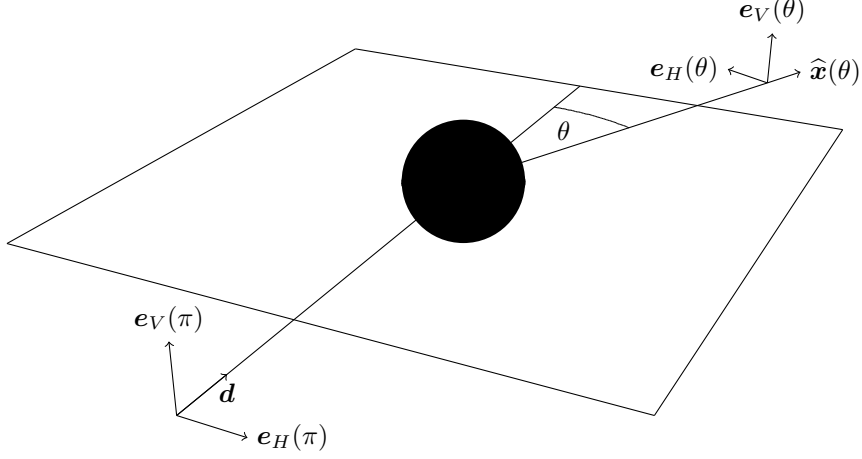


Fig. 1 Schematic showing vertical (V) and horizontal (H) polarization with respect to the scattering plane for an incident wave with direction \mathbf{d} and a receiver in the direction $\hat{\mathbf{x}}(\theta)$.

To demonstrate the correctness of our fully-discrete algorithm for the all-frequency stable system (47), in Tables 1–4 we tabulate the relative error

$$\text{ERR}_{\text{Mie},n} = \frac{\|\mathbf{E}_{\infty,n}(\theta) - \mathbf{E}_{\infty,\text{ref}}(\theta)\|_{\infty}}{\|\mathbf{E}_{\infty,\text{ref}}(\theta)\|_{\infty}} \quad (109)$$

for scattering of H-polarized incident plane waves by the unit sphere. The reference solution $\mathbf{E}_{\infty,\text{ref}}$ is computed to high precision using Wiscombe’s Mie series code [30]. In practice, the maximum norms in (109) are approximated discretely using more than 1200 evenly spaced points $\theta \in [0, 2\pi]$.

For non-spherical scatterers we demonstrate the correctness of our algorithm using the reciprocity relation [6, Theorem 6.30]. In particular, in Tables 5–9 we tabulate the relative error

$$\text{ERR}_{\text{RP},n} = \frac{\|\mathbf{e}_H(\theta) \cdot \mathbf{E}_{\infty,n}(\theta; \theta') - \mathbf{e}_H(\theta') \cdot \mathbf{E}_{\infty,n}(\theta'; \theta)\|_{\infty}}{\|(\mathbf{E}_{\infty,n}(\theta; \theta') \cdot \mathbf{E}_{\infty,n}(\theta'; \theta))^{1/2}\|_{\infty}}, \quad (110)$$

which measures the residual in the reciprocity relation. In (110) we denote by $\mathbf{E}_{\infty,n}(\cdot; \theta')$ the far field induced by the H-polarized incident wave with direction $\mathbf{d} = -(\sin \theta', 0, \cos \theta')^T$. The norms in (110) are over $(\theta, \theta') \in [0, 2\pi] \times [0, 2\pi]$ and are approximated discretely using more than 1200×1200 points. The tabulated results demonstrate the superalgebraic convergence established by the numerical analysis in (78). In particular, high order accuracy is attained with only a small increase in the discretization parameter n (with r in (78) sufficiently large due to smoothness of the test particles). In Table 10 we tabulate the CPU time and memory for computing the non-convex penetrable Chebyshev particle results in Tables 7–9, demonstrating that the spectral accuracy of our fully-discrete algorithm facilitates simulation of the low

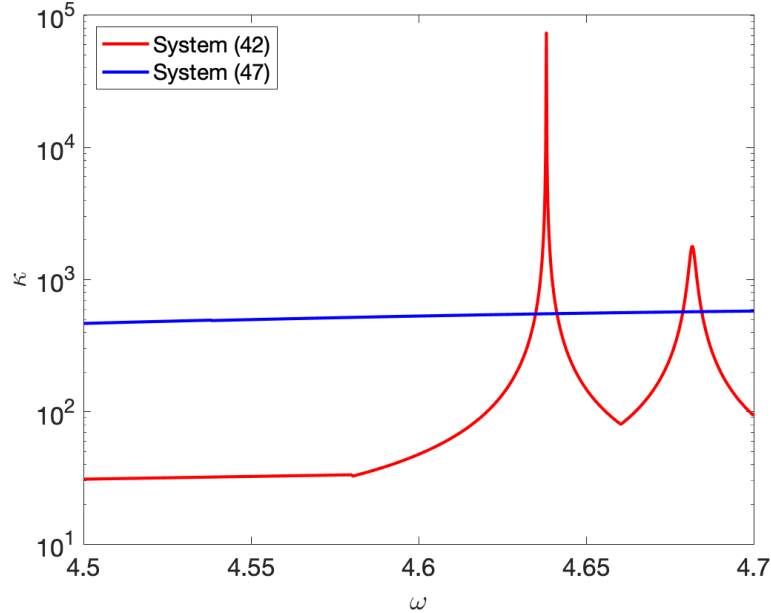


Fig. 2 Condition number κ of the matrix in systems (42) (without stabilization) and (47) (with stabilization) for a dielectric unit sphere with refractive index $\nu = 1.303324617806156$ and frequency ω .

to medium-frequency Maxwell model in three dimensions to high-accuracy even using laptops with multicore processors.

For convenient visualization of the reciprocity relation, in Figures 3–5 we plot the radar cross section σ_{HH} of the Chebyshev particle in its original orientation, and rotated by an angle $\pi/2$ clockwise about the y -axis. Following [4, Page 314], the coincidence of the radar cross sections at $\theta = \pi/2$ demonstrates that the computed solutions satisfy the reciprocity relation (using the symmetry of the Chebyshev particle about the xy -plane).

In Figure 6 we demonstrate the visual agreement of the radar cross section σ_{HH} computed using our code and using Mishchenko’s null-field-method code (downloaded from [32] and documented in [33]) for spheroids with aspect ratio $\rho = 2$ and electromagnetic size $s = 8$. In Figure 7 we demonstrate similar agreement for spheroids with aspect ratio $\rho = 5$ and electromagnetic size $s = 1$. The null field method is not able to compute the radar cross section for spheroids with such large aspect ratio $\rho = 5$ and electromagnetic size $s = 8$ because it exhibits numerical instability for large aspect ratio scatterers and large electromagnetic sizes [26]. The target accuracy of the computations using Mishchenko’s code is about 10^{-3} .

The induced electric field \mathbf{E}^{\pm} is given by the surface integral representation [11, Equation (6.1)] (see also [15, Equations (2.8)–(2.9)]) and computed in a similar way to the far-field. In Figure 8 we visualize the total field $|\text{Re } \mathbf{E}_{\text{tot},n}(\mathbf{x})|$ and the relative error in the induced electric field for Chebyshev particles with electromagnetic size $s = 1$ and $s = 8$ illuminated by an H-polarized incident plane wave. Because the true

	$\nu = 1.584$	$\nu = 1.5 + 0.02i$	$\nu = 1.0925 + 0.248i$
n	ERR _{Mie,n}	ERR _{Mie,n}	ERR _{Mie,n}
1	1.00e+00	9.44e-01	7.06e-01
2	4.21e-10	4.27e-10	4.44e-10
3	4.13e-10	4.88e-10	6.94e-10

Table 1 Scattering by a **sphere** with diameter $10^{-6}\lambda$.

induced field is not known for this geometry, the relative error at \mathbf{x} is approximated by

$$\text{ERR}_{\pm,n}(\mathbf{x}) = \frac{|\mathbf{E}_n^{\pm}(\mathbf{x}) - \mathbf{E}_{n+10}^{\pm}(\mathbf{x})|}{|\mathbf{E}_{n+10}^{\pm}(\mathbf{x})|}$$

where \mathbf{E}_n^{\pm} denotes the computed induced electric field in the exterior and interior respectively, and we use the solution computed with increased parameter $n+10$ as the reference solution. As \mathbf{x} approaches the boundary ∂D , the accuracy is compromised due to the near-singularity in the kernel of the near-field potentials associated with surface currents. To ensure high-order accuracy in the numerical evaluation of near-fields very close to the boundary, it is necessary to develop specialized techniques for accurately evaluating these near-singular surface potential integrals. Techniques such as those described in [34, 35] can be used in conjunction with our high-order accurate surface currents. However, we have not yet implemented these sophisticated techniques for near-field evaluations. Using our own approach with approximations induced by the operator \mathcal{L}_n with high-order convergence property (71), as observed in Figure 8, we obtain about five-digits accuracy even very close to the boundary.

We close the numerical experiments with results for plasmonic and eddy current (very low frequency) material parameters. We recall that our continuous and discrete model analyses are not applicable for plasmonic material parameters. In Tables 11–12 we explore the eddy current regime considered in [36] by tabulating the relative error (109) for unit spheres with refractive indices having modulus between 10^2 and 10^4 , and argument $\pi/4$. For these results we use our own Mie code. In Figure 9 we plot the 1-norm condition number of the matrix representing $I + \tilde{\mathbf{M}}$ for a unit sphere scatterer with material properties described by

$$x = \frac{1 + \hat{\epsilon}}{1 - \hat{\epsilon}}, \quad (111)$$

where $\hat{\epsilon} = \epsilon_-/\epsilon_+$ is the relative permittivity (which, in our examples, is equal to the square of the refractive index ν). The condition number is computed for refractive indices on the path shown in Figure 10 using the same methodology used for Figure 2. The same path is used in [34, Figure 10], and the eddy current region is characterised by x near 1, whilst the plasmonic regime is characterised by $x \in (-1, 1)$. Finally, in Figure 11 we visualize the total field $|\text{Re } \mathbf{E}_{\text{tot},n}(\mathbf{x})|$ for a Chebyshev particle with electromagnetic size $s = 2$ illuminated by an H-polarized incident plane wave. The refractive index is $\nu = 1.088025734989757i$, so that the relative permittivity is negative, leading to plasmonic surface waves.

	$\nu = 1.584$	$\nu = 1.5 + 0.02i$	$\nu = 1.0925 + 0.248i$
n	$\text{ERR}_{\text{Mie},n}$	$\text{ERR}_{\text{Mie},n}$	$\text{ERR}_{\text{Mie},n}$
1	1.00e+00	9.44e-01	7.06e-01
2	6.92e-07	6.64e-07	5.56e-07
3	1.01e-12	9.36e-13	8.26e-13

Table 2 Scattering by a **sphere** with diameter $10^{-3}\lambda$.

	$\nu = 1.584$	$\nu = 1.5 + 0.02i$	$\nu = 1.0925 + 0.248i$
n	$\text{ERR}_{\text{Mie},n}$	$\text{ERR}_{\text{Mie},n}$	$\text{ERR}_{\text{Mie},n}$
5	8.04e-03	7.35e-03	6.72e-03
10	1.25e-09	1.17e-09	1.26e-09
15	1.03e-09	1.02e-09	1.61e-09

Table 3 Scattering by a **sphere** with diameter λ .

	$\nu = 1.584$	$\nu = 1.5 + 0.02i$	$\nu = 1.0925 + 0.248i$
n	$\text{ERR}_{\text{Mie},n}$	$\text{ERR}_{\text{Mie},n}$	$\text{ERR}_{\text{Mie},n}$
30	1.46e-01	1.27e-01	5.79e-04
35	1.91e-03	1.59e-04	3.15e-07
40	1.98e-08	2.18e-10	5.65e-11

Table 4 Scattering by a **sphere** with diameter 8λ .

	$\nu = 1.584$	$\nu = 1.5 + 0.02i$	$\nu = 1.0925 + 0.248i$
n	$\text{ERR}_{\text{RP},n}$	$\text{ERR}_{\text{RP},n}$	$\text{ERR}_{\text{RP},n}$
Aspect ratio 2			
5	1.61e-03	1.44e-03	1.52e-03
10	3.76e-07	3.37e-07	6.31e-07
15	1.39e-09	1.30e-09	1.45e-09
Aspect ratio 3			
5	1.61e-03	1.27e-03	1.74e-03
15	2.84e-07	2.87e-07	3.66e-07
25	1.52e-10	1.54e-10	1.97e-10
Aspect ratio 4			
5	2.00e-03	1.64e-03	2.72e-03
15	2.95e-06	3.14e-06	4.81e-06
25	9.49e-09	1.01e-08	1.55e-08
Aspect ratio 5			
10	9.93e-05	1.33e-04	5.27e-04
20	5.23e-07	7.24e-07	3.32e-06
30	4.16e-09	6.03e-09	3.21e-08

Table 5 Scattering by a **spheroid** with diameter λ .

	$\nu = 1.584$	$\nu = 1.5 + 0.02i$	$\nu = 1.0925 + 0.248i$
n	$\text{ERR}_{\text{RP},n}$	$\text{ERR}_{\text{RP},n}$	$\text{ERR}_{\text{RP},n}$
Aspect ratio 2			
20	4.62e-01	3.77e-01	7.99e-01
30	6.33e-02	1.76e-02	8.53e-04
40	9.33e-05	4.36e-07	8.48e-12
Aspect ratio 3			
20	2.80e-01	3.93e-01	5.73e-01
30	4.72e-02	2.64e-02	1.23e-03
40	9.37e-05	1.76e-06	2.71e-11
Aspect ratio 4			
20	3.82e-01	2.47e-01	4.46e-01
30	7.78e-02	2.88e-02	1.00e-03
40	1.36e-04	3.52e-06	1.02e-10
Aspect ratio 5			
20	2.11e-01	1.95e-01	4.11e-01
30	4.23e-02	3.07e-02	6.80e-04
40	1.45e-04	1.91e-06	2.05e-09

Table 6 Scattering by a **spheroid** with diameter 8λ .

	$\nu = 1.584$	$\nu = 1.5 + 0.02i$	$\nu = 1.0925 + 0.248i$
n	$\text{ERR}_{\text{RP},n}$	$\text{ERR}_{\text{RP},n}$	$\text{ERR}_{\text{RP},n}$
20	9.36e-03	9.26e-03	1.25e-02
30	5.21e-04	6.04e-04	1.23e-03
40	1.03e-04	9.92e-05	1.24e-04

Table 7 Scattering by a **Chebyshev particle** with diameter λ .

	$\nu = 1.584$	$\nu = 1.5 + 0.02i$	$\nu = 1.0925 + 0.248i$
n	$\text{ERR}_{\text{RP},n}$	$\text{ERR}_{\text{RP},n}$	$\text{ERR}_{\text{RP},n}$
40	1.64e-03	8.77e-04	2.00e-04
50	7.49e-05	5.15e-05	2.48e-05
60	1.02e-05	6.00e-06	4.01e-06

Table 8 Scattering by a **Chebyshev particle** with diameter 4λ .

	$\nu = 1.584$	$\nu = 1.5 + 0.02i$	$\nu = 1.0925 + 0.248i$
n	$\text{ERR}_{\text{RP},n}$	$\text{ERR}_{\text{RP},n}$	$\text{ERR}_{\text{RP},n}$
60	7.89e-03	1.19e-03	1.26e-02
70	4.39e-04	8.74e-05	4.96e-04
80	2.69e-05	5.16e-06	2.09e-05

Table 9 Scattering by a **Chebyshev particle** with diameter 8λ .

n	memory	CPU time
20	107 MB	34.7 s
40	1.52 GB	6.8 min
60	7.43 GB	40.4 min
80	23.09 GB	3.0 h

Table 10 Memory required to store the discretization matrix and CPU wall time for computing the far-field for 1202 distinct incident plane waves for the non-convex Chebyshev particles (with high-order accuracy indicated in Tables 7–9). CPU times are in parallel on a single compute node with a 2.8 GHz Intel Xeon 8562Y 32-cores processor.

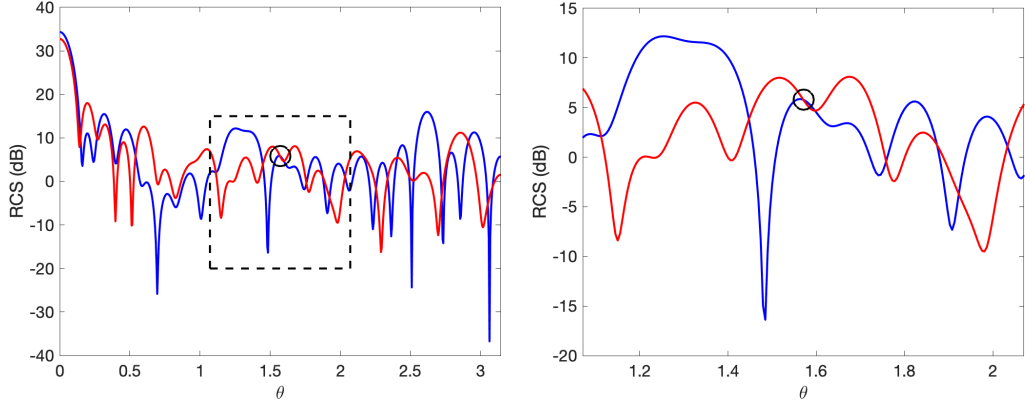


Fig. 3 Visualization of the radar cross section (HH-polarization) computed with $n = 80$ of a Chebyshev particle with refractive index $\nu = 1.584$ and electromagnetic size $s = 8$ in original orientation (blue) and $\pi/2$ -rotated orientation (red). Coincidence of the curves at $\theta = \pi/2$ is marked by a \circ . The right figure shows a close-up of the region indicated by the box in the left figure.

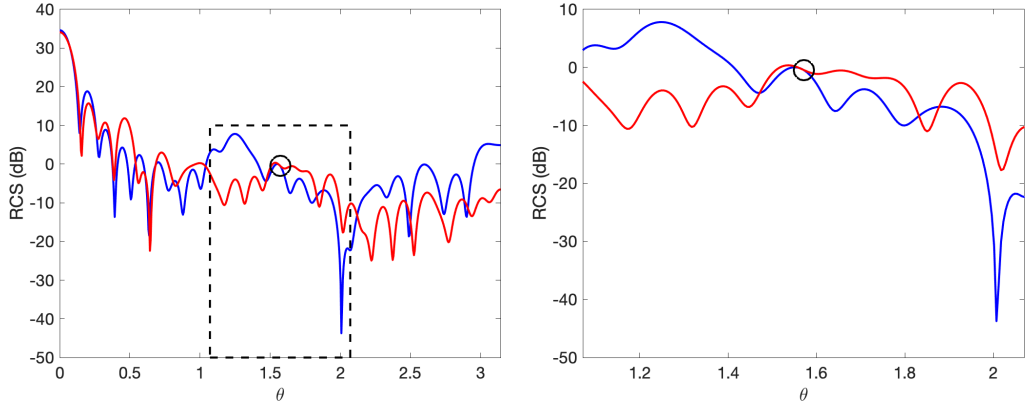


Fig. 4 Visualization of the radar cross section (HH-polarization) computed with $n = 80$ of a Chebyshev particle with refractive index $\nu = 1.5 + 0.02i$ and electromagnetic size $s = 8$ in original orientation (blue) and $\pi/2$ -rotated orientation (red). Coincidence of the curves at $\theta = \pi/2$ is marked by a \circ . The right figure shows a close-up of the region indicated by the box in the left figure.

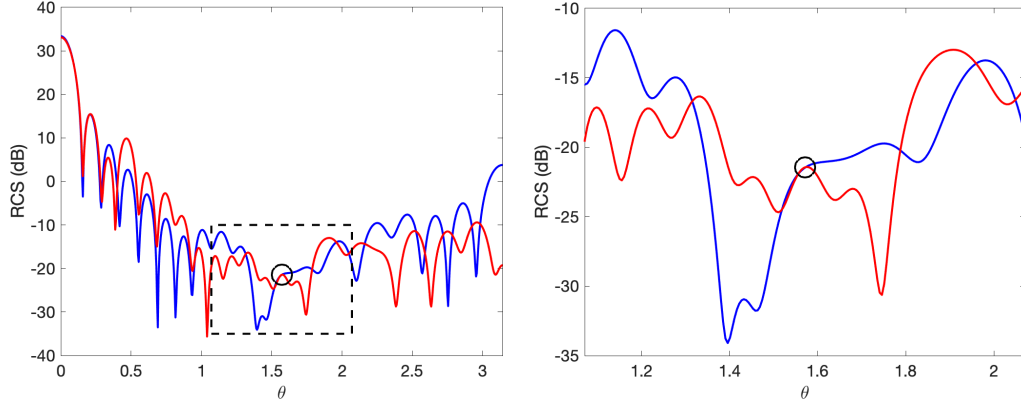


Fig. 5 Visualization of the radar cross section (HH-polarization) computed with $n = 80$ of a Chebyshev particle with refractive index $\nu = 1.0925 + 0.248i$ and electromagnetic size $s = 8$ in original orientation (blue) and $\pi/2$ -rotated orientation (red). Coincidence of the curves at $\theta = \pi/2$ is marked by a \circ . The right figure shows a close-up of the region indicated by the box in the left figure.

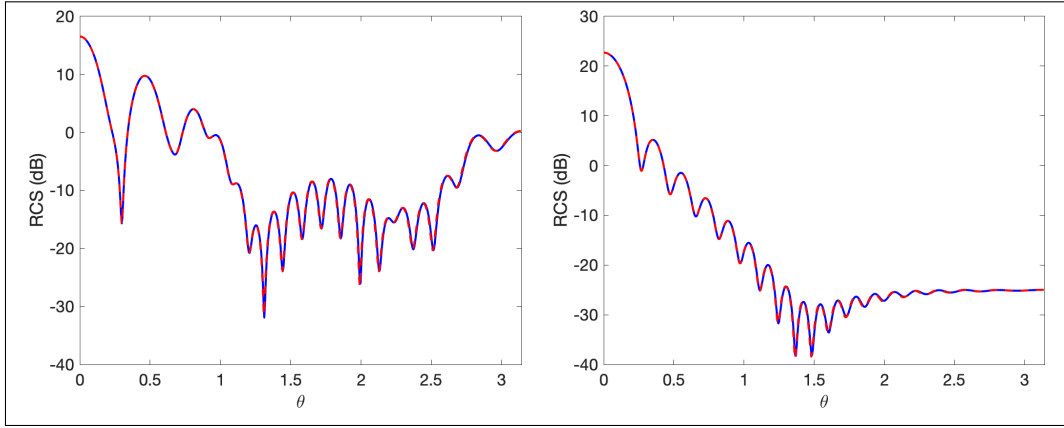


Fig. 6 Visualization of the radar cross section (HH-polarization) computed with $n = 50$ of a spheroid with aspect ratio 2, refractive index $\nu = 1.584$ (left) and $\nu = 1.0925 + 0.248i$ (right), and electromagnetic size $s = 8$ computed using this algorithm (blue) and Mishchenko's code (red dashed).

	$\nu = 10^2(1 + i)$	$\nu = 10^3(1 + i)$	$\nu = 10^4(1 + i)$
n	$\text{ERR}_{\text{Mie},n}$	$\text{ERR}_{\text{Mie},n}$	$\text{ERR}_{\text{Mie},n}$
2	4.09e-07	3.97e-05	8.62e-05
3	1.50e-07	5.22e-06	5.79e-06
4	3.26e-09	5.58e-07	2.32e-06

Table 11 Scattering by a plasmonic **sphere** with diameter $10^{-5}\lambda$.

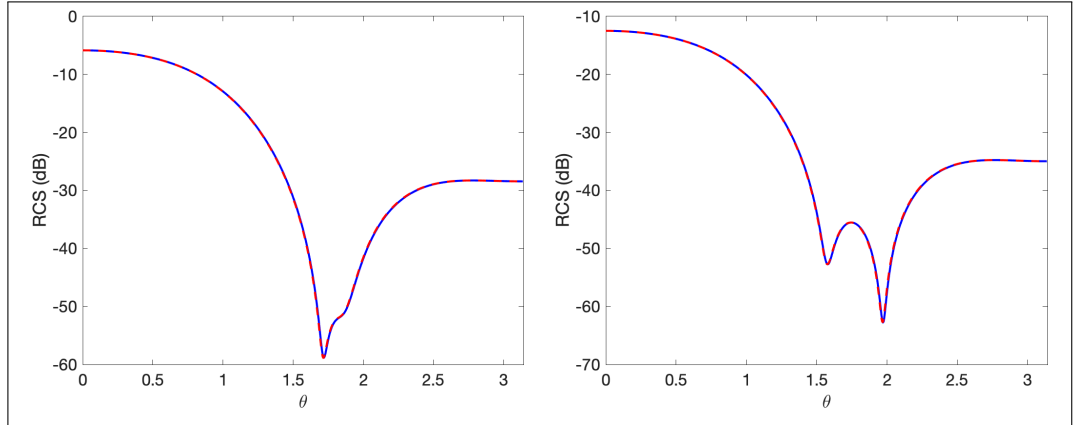


Fig. 7 Visualization of the radar cross section (HH-polarization) computed with $n = 30$ of a spheroid with aspect ratio 5, refractive index $\nu = 1.584$ (left) and $\nu = 1.0925 + 0.248i$ (right), and electromagnetic size $s = 1$ computed using this algorithm (blue) and Mishchenko's code (red dashed).

	$\nu = 10^2(1 + i)$	$\nu = 10^3(1 + i)$	$\nu = 10^4(1 + i)$
n	$\text{ERR}_{\text{Mie},n}$	$\text{ERR}_{\text{Mie},n}$	$\text{ERR}_{\text{Mie},n}$
2	3.95e-05	2.64e-03	2.65e+00
3	1.50e-08	5.91e-08	3.76e-02
4	4.48e-10	2.86e-08	2.41e-04

Table 12 Scattering by a plasmonic **sphere** with diameter $10^{-4}\lambda$.

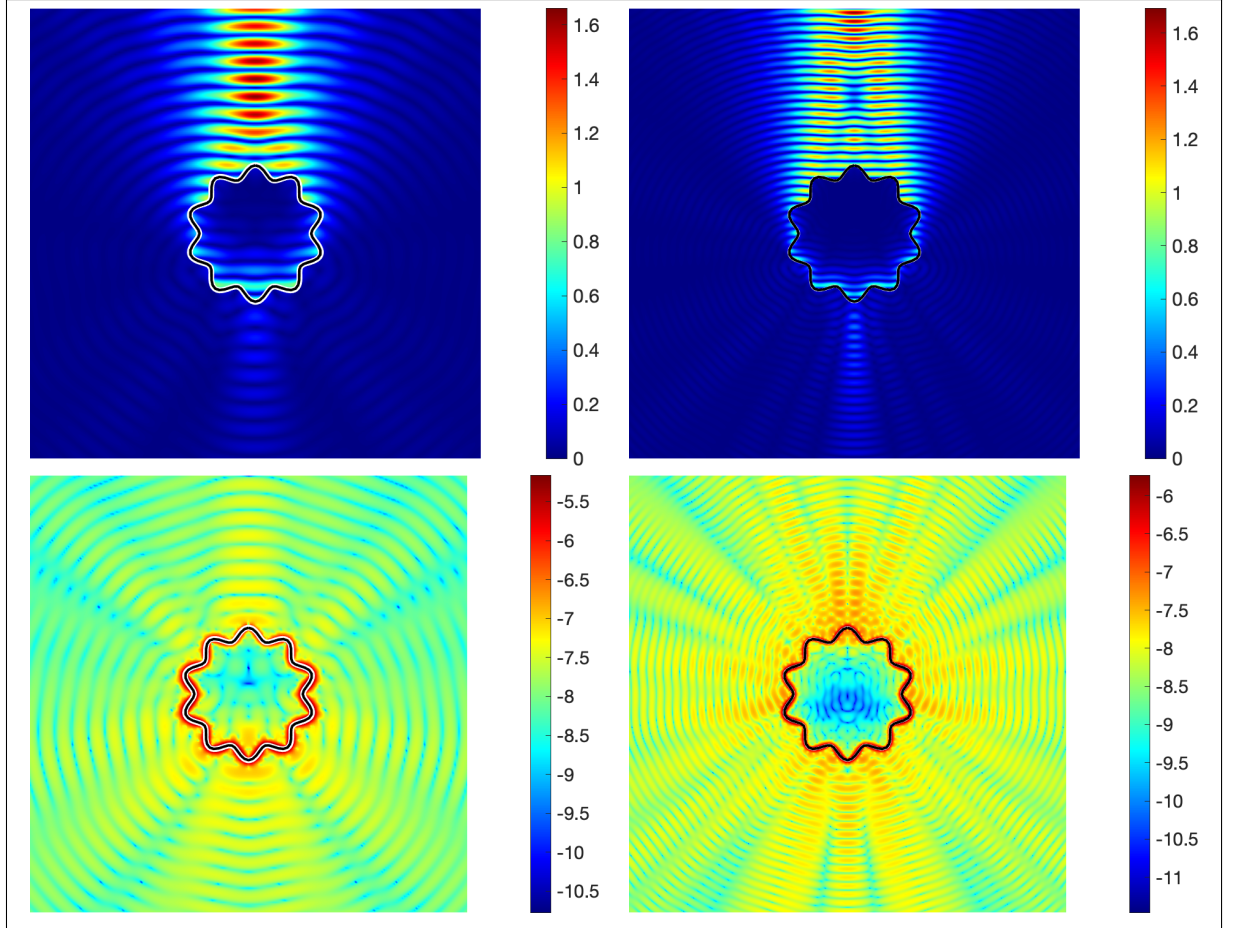


Fig. 8 Visualization of the interior and exterior total electric fields $|\text{Re } \mathbf{E}_{\text{tot},n}|$ induced by a H-polarized plane wave striking a Chebyshev particle with refractive index $\nu = 1.0925 + 0.248i$ and electromagnetic size $s = 4$ (top left) and $s = 8$ (top right) computed with $n = 80$ and $n = 110$ respectively. The corresponding relative error $\log_{10}(\text{ERR}_{\pm,n}(\mathbf{x}))$ is visualized (bottom left and right).

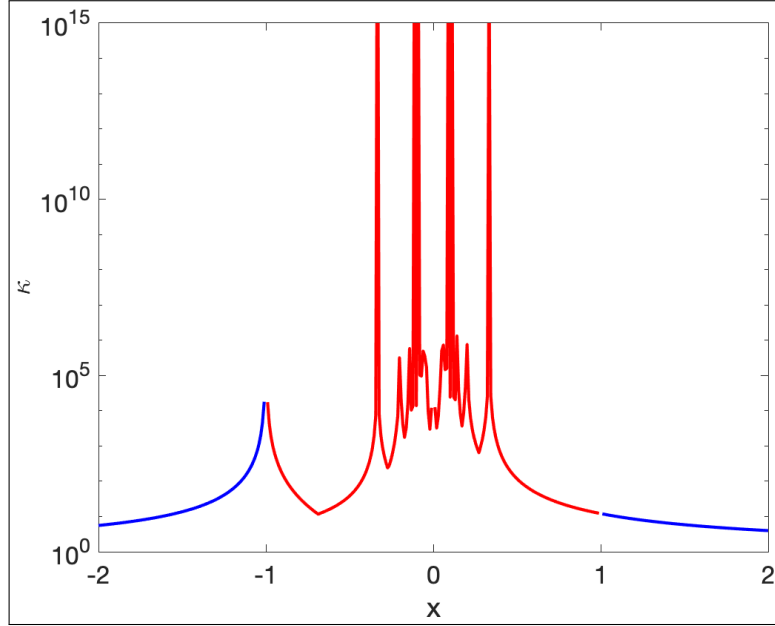


Fig. 9 Condition number κ of the matrix in system (47) (with stabilization) for a unit sphere with size 10^{-6} against $x = (1 + \hat{\epsilon}) / (1 - \hat{\epsilon})$ where $\hat{\epsilon} = \epsilon_- / \epsilon_+$ is the relative permittivity of the scatterer. The path along which the condition number is computed is shown in Figure 10. The stability analysis in this article applies to the dielectric region $x \in (-\infty, -1) \cup (1, \infty)$ (blue line). The plasmonic region is $x \in (-1, 1)$ (red line).

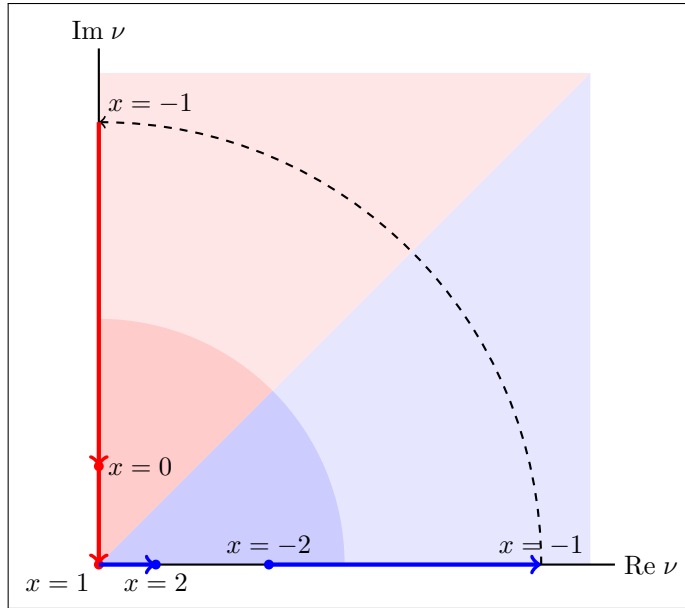


Fig. 10 Schematic showing the path along which the condition number is plotted in Figure 9. The dielectric and absorbing region is marked by blue shading, the plasmonic region by red shading, and the Eddy current region where $|\nu|$ is large by light shading.

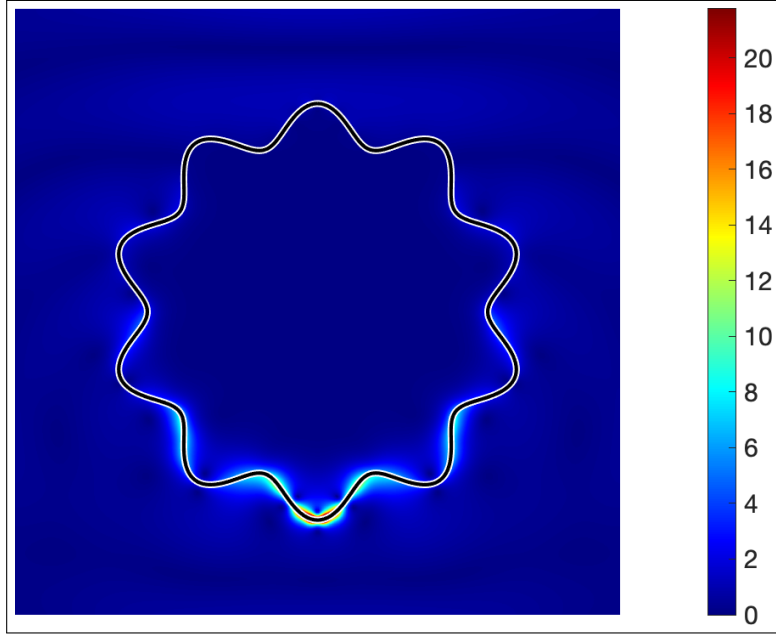


Fig. 11 Visualization of the interior and exterior total electric fields $|\text{Re} \mathbf{E}_{\text{tot},n}|$ induced by a H-polarized plane wave striking a *plasmonic* Chebyshev particle with refractive index $\nu = 1.088025734989757i$ and electromagnetic size $s = 2$ computed with $n = 100$.

A Singularity of standard coupling approach

Proposition A.1. *Let H be a Hilbert space. Assume that either H is finite dimensional with $\dim H \geq 2$ or H is separable. There exist two compact linear operators $\mathbb{M}, \mathbb{J} : H \rightarrow H$ such that $N(\mathbb{J}) \cap N(\mathbb{I} + \mathbb{M}) = \{0\}$ and, for every $\xi \in \mathbb{C}$, $\mathbb{I} + \mathbb{M} + \xi\mathbb{J}$ is singular.*

Proof. In dimension 2 we set

$$\mathbb{I} + \mathbb{M} = \begin{pmatrix} 1 & 0 \\ 0 & 0 \end{pmatrix}, \quad \mathbb{J} = \begin{pmatrix} 0 & 1 \\ 0 & 0 \end{pmatrix}$$

It is clear that $\mathbb{I} + \mathbb{M} + \xi\mathbb{J}$ is singular, for any $\xi \in \mathbb{C}$. Generalizing this example to higher dimensions is trivial using block matrices.

Let H be a separable Hilbert space and $\{e_i : i \in \mathbb{N}, i \geq 1\}$ a Hilbert basis of H . Define \mathbb{M} by

$$\mathbb{M}e_i = \begin{cases} -e_i, & \text{for } i = 2, \\ 0, & \text{for } i \neq 2, \end{cases}$$

and \mathbb{J} by

$$\mathbb{J}e_i = \begin{cases} e_1, & \text{for } i = 2, \\ 0, & \text{for } i \neq 2. \end{cases}$$

A simple calculation can show that $N(\mathbb{J}) \cap N(\mathbb{I} + \mathbb{M}) = \{0\}$ and $(\mathbb{I} + \mathbb{M} + \xi\mathbb{J})(\xi e_1 - e_2) = 0$ for any $\xi \in \mathbb{C}$. \square

Remark 11. *In dimension three or higher, or in a separable Hilbert space, $\mathbb{I} + \mathbb{M} + \xi\mathbb{J}$ may be singular for all $\xi \in \mathbb{C}$, even if both \mathbb{M} and \mathbb{J} are symmetric, compact, and $N(\mathbb{J}) \cap N(\mathbb{I} + \mathbb{M}) = \{0\}$. In dimension 3, set*

$$\mathbb{I} + \mathbb{M} = \begin{pmatrix} 0 & 0 & 1 \\ 0 & 0 & 1 \\ 1 & 1 & 0 \end{pmatrix}, \quad \mathbb{J} = \begin{pmatrix} 1 & 0 & 0 \\ 0 & -1 & 0 \\ 0 & 0 & 0 \end{pmatrix}.$$

We note that $N(\mathbb{J}) \cap N(\mathbb{I} + \mathbb{M}) = \{0\}$ and yet $(\mathbb{I} + \mathbb{M} + \xi\mathbb{J})(1, -1, -\xi) = 0$, for all $\xi \in \mathbb{C}$. This counterexample can be easily extended to any separable Hilbert space.

Acknowledgments. The first two authors gratefully acknowledge the support of the Australian Research Council (ARC) Discovery Project Grant (DP220102243). MG was also supported by the Simons Foundation through grant 518882. SCH thanks the Isaac Newton Institute for Mathematical Sciences for hospitality during the program Mathematical Theory and Applications of Multiple Wave Scattering and acknowledges support of the EPSRC (Grant Number EP/R014604/1) and the Simons Foundation.

Declarations

Conflict of interest: The authors declare no competing interests.

References

- [1] Cheney, M., Borden, B.: Fundamentals of Radar Imaging. SIAM, (2009)
- [2] Hulst, H.C.: Light Scattering by Small Particles. Dover Publications Inc., (1981)
- [3] Kristensson, G.: Scattering of Electromagnetic Waves by Obstacles. SciTech, (2016)
- [4] Rother, T., Kahnert, M.: Electromagnetic Wave Scattering on Nonspherical Particles: Basic Methodology and Simulations, 2nd edn. Springer, (2013)
- [5] Costabel, M., Louër, F.L.: On the Kleinman–Martin integral equation method for electromagnetic scattering by a dielectric body. *SIAM J. Appl. Math.* **71**, 635–656 (2011)
- [6] Colton, D., Kress, R.: Inverse Acoustic and Electromagnetic Scattering Theory, 4th edn. Springer, Cham, Switzerland (2019)
- [7] Nédélec, J.-C.: Acoustic and Electromagnetic Equations. Springer, New York (2001)
- [8] Müller, C.: Zur Mathematischen Theorie Elektromagnetischer Schwingungen vol. 3, p. 23. Deutsche Akademie, Berlin (1945/46)
- [9] Müller, C.: Foundations of the Mathematical Theory of Electromagnetic Waves. Springer, Berlin Heidelberg (1969)
- [10] Buffa, A., Ammari, H., Nédélec, J.-C.: A justification of eddy currents model for the maxwell equations. *SIAM Journal on Applied Mathematics* **60**(5), 1805–1823 (2000)
- [11] Ganesh, M., Hawkins, S.C., Volkov, D.: An all-frequency weakly-singular surface integral equation for electromagnetism in dielectric media: Reformulation and well-posedness analysis. *Journal of Mathematical Analysis and Applications* **412**(1), 277–300 (2014)
- [12] Maue, A.-W.: Formulierung eines allgemeinen beugungsproblems durch eine integral-gleichung. *Z. Physik* **126**, 601–618 (1949)
- [13] Epstein, C., Greengard, L.: Debye sources and the numerical solution of the time harmonic Maxwell equations. *Comm. Pure Appl. Math.* **63**, 413–463 (2009)
- [14] Epstein, C., Greengard, L., O’Neal, M.: Debye sources and the numerical solution of the time harmonic Maxwell equations II. *Comm. Pure Appl. Math.* **66**, 753–789 (2013)
- [15] Ganesh, M., Hawkins, S.C., Volkov, D.: An efficient algorithm for a class of

- stochastic forward and inverse Maxwell models in \mathbb{R}^3 . *J. Comput. Phys.* **398**, 10881 (2019)
- [16] Helsing, J., Karlsson, A., Roseñ, A.: Comparison of integral equations for the maxwell transmission problem with general permittivities. *Adv. Comput. Math.* **47**, 76–32 (2021)
- [17] Ylä-Oijala, P., Taskinen, M.: Well-conditioned Müller formulation for electromagnetic scattering by dielectric objects. *IEEE Antennas and Propagation* **53**, 3316–3325 (2005)
- [18] Taskinen, M., Vanska, S.: Current and charge integral equation formulations and Picard’s extended Maxwell system. *IEEE Antennas and Propagation* **55**, 3495–3503 (2007)
- [19] Ganesh, M., Hawkins, S.C.: A spectrally accurate algorithm for electromagnetic scattering in three dimensions. *Numer. Algorithms* **43**, 25–60 (2006)
- [20] Costabel, M.: Boundary integral operators on Lipschitz domains: Elementary results. *SIAM J. Math. Anal.* **19**, 613–626 (1988)
- [21] Colton, D., Kress, R.: *Integral Equation Methods in Scattering Theory*. SIAM, Philadelphia (2013)
- [22] Maz’ya, V.G.: Boundary integral equations. In: *Analysis IV: Linear and Boundary Integral Equations*. Springer, Berlin Heidelberg (1991)
- [23] Nédélec, J.-C.: *Acoustic and Electromagnetic Equations: Integral Representations for Harmonic Problems* vol. 144. Springer, (2001)
- [24] Sauter, S.A., Schwab, C.: *Boundary Element Methods*. Springer, (2011)
- [25] Benzi, M., Golub, G.H., Liesen, J.: Numerical solution of saddle point problems. *Acta numerica* **14**, 1–137 (2005)
- [26] Mishchenko, M.I., Travis, L.D.: T-matrix computations of light scattering by large spheroidal particles. *Opt. Commun.* **109**, 16–21 (1994)
- [27] Kahnert, M., Rother, T.: Modeling optical properties of particles with small-scale surface roughness: combination of group theory with a perturbation approach. *Opt. Express* **19**, 11138–11151 (2011)
- [28] Rother, T., Schmidt, K., Wauer, J., Shcherbakov, V., Gayet, J.-F.: Light scattering on Chebyshev particles of higher order. *Appl. Opt.* **45**, 6030–6037 (2006)
- [29] Sloan, I.H., Womersley, R.S.: Constructive polynomial approximation on the sphere. *Jornal of Approximation Theory* (2000)

- [30] Wiscombe, W.J.: Improved Mie scattering algorithms. *Applied Optics* **19**, 1505–1509 (1990)
- [31] Higham, N.J.: Fortran codes for estimating the one-norm of a real or complex matrix, with applications to condition estimation. *ACM Trans. Math. Soft.*, 381–396 (1988)
- [32] Mishchenko, M.I. <http://www.giss.nasa.gov/staff/mmishchenko/tmatrix/>
- [33] Mishchenko, M.I.: Calculation of the amplitude matrix for a nonspherical particle in a fixed orientation. *Appl. Opt.* **39**, 1026–1031 (2000)
- [34] Helsing, J., Ojala, R.: On the evaluation of layer potentials close to their sources. *J. Comput. Phys.* **227**, 2899–2921 (2008)
- [35] Klinteberg, L., Barnett, A.: Accurate quadrature of nearly singular line integrals in two and three dimensions by singularity swapping. *BIT Numer. Math.* **61**, 83–118 (2021)
- [36] Helsing, J., Karlsson, A., Rosén, A.: An efficient full-wave solver for eddy currents. *Comput. Math. Appl.* **128**, 145–162 (2022)